**Title**
AIRTOUCH: A NOVEL SINGLE LAYER 3D TOUCH SENSING SYSTEM FOR HUMAN/MOBILE DEVICE INTERACTIONS



**Author**
Du, Li Du

**Publication Date**
2016

Peer reviewed|Thesis/dissertation

UNIVERSITY OF CALIFORNIA
Los Angeles

# AIRTOUCH: A NOVEL SINGLE LAYER 3D TOUCH SENSING SYSTEM FOR HUMAN/MOBILE DEVICE INTERACTIONS

A dissertation submitted in partial satisfaction of the

requirements for the degree Doctor of Philosophy

in Electrical Engineering

by

Li Du

2016

# ABSTRACT OF THE DISSERATION

AIRTOUCH: A NOVEL SINGLE LAYER 3D TOUCH SENSING SYSTEM FOR HUMAN/MOBILE DEVICE INTERACTIONS

by

Li Du

Doctor of Philosophy in Electrical Engineering

University of California, Los Angeles, 2016

Professor Mau-Chung Frank Chang, Chair

Touch sensing has been widely implemented as a main methodology to bridge human and machine interactions. The traditional touch sensing range is two dimensional and therefore limits the user experience. The required physical contact inherent of the technology creates several disadvantages, including unresponsiveness due to wet fingers, and unavoidable fingerprint residue on the screen surface.

To overcome these limitations, we propose a novel 3D contactless touch sensing system called Airtouch System, which improves user experience by remotely detecting single/multi-finger position. A single layer touch panel with triangular electrodes is used to achieve 3D multi-touch detection capability as well as manufacturing cost reduction. A lumped model of the touch panel

is proposed to model the touch panel property and define the system specification. The hardware part of the proposed 3D touch sensor uses correlated double sampling (CDS) to achieve a high sensing resolution in Z direction and employs bootstrapping circuitry to reduce the mobile screen's inter-channel-coupling effects. Additionally, to reduce chip area and assembly, the sensing oscillator is implemented with inverter-based active resonators instead of using either on or off chip inductors. The prototyped 3D touch sensor is fabricated using 65-nm CMOS process technology and consumes an area of $2mm^2$.

To detect the finger position in space, a new algorithm for finger position estimation is created with grouping filter invented to reduce system background noise. The algorithm is proposed to eliminate the fringing capacitance effect and achieve accurate finger position estimation. EM simulation proved that by taking account of fringing capacitance effect, the proposed algorithm reduced the systematic error by 11dB in the horizontal position detection. Accurate Z direction detection is achieved through using 2nd order polynomial curve to fit the EM model and compensate the non-linear fringing capacitance effect. The proposed system's hardware circuit consumes 2.3mW and is fully compatible with existing mobile device environments. A prototype is built to demonstrate that the system can successfully detect finger movement in a vertical direction up to 6cm and achieve a horizontal resolution up to 0.6cm at 1cm finger-height. As a new interface for human and machine interactions, this system offers great potential in 3D gesture recognition for small-sized electronics and advanced human interactive games for mobile devices.

The dissertation of Li Du is approved.

Kung Yao

Wentai Liu

Xiaochun Li

Mau-Chung Frank Chang, Committee Chair

University of California, Los Angeles

2016

# Table of Contents

# LIST OF ACORNYMS

| Acronyms | Meaning | Acronyms | Meaning |
|---|---|---|---|
| 2D | Two Dimensional | HTC | Hong Da Guo ji Dian Zi Corporation, Taiwan |
| 3D | Three Dimensional | JPL | Jet Propulsion Laboratory |
| APR | Acoustic Pulse Recognition | LSB | least significant bit |
| ADC | Analog to Digital Converter | MSB | most significant bit |
| BCDS | Bootstrapped Correlated Double Sampling | MCU | Mic-controller Unit |
| CDS | Correlated Double Sampling | PC | Personal Computor |
| DAC | Digital to Analog Converter | PCB | Printed Circuit Board |
| ESD | Electrostatic Discharge | RX | Receiver |
| EM | Electric Magnetic | SAR | Successive Approximation Register |
| HID | Human Interface Device | SAW | Surface Acoustic Wave |
| GUI | Graphical User Interface | SOC | System On Chip |
| HMI | Human Machine Interface | TSMC | Taiwan Semiconductor Manufacturing Company |
| ITO | Indium Tin Oxide | TX | Transceiver |
| HSEL | High Speed Electronics Laboratory | USART | Universal Synchronous/Asynchronous Receiver/Transmitter |

# LIST OF FIGURES

# LIST OF TABLES

# ACKNOWLEDGEMENT

No great journey can be completed alone. My long and checkered UCLA academic career is certainly no exception. I'm blessed to have met so many great individuals throughout my UCLA journey and I'd like to take this opportunity to acknowledge them.

First, I would like to express my deepest gratitude to Prof. Frank Chang. He provides me with the inspiration and motivation in this project as well as valuable advice and guidance. During numerous meetings with him, reporting and discussing the progress of the dissertation, I learnt quite a lot about how to independently guide work on research in a productive manner and how to solve industry technical problems using system-level way of thinking. I would also like to thank Professor Kung Yao, Professor Wentai Liu and Professor Xiaochun Li for taking their time to serve on my committee.

I would also like to thank Dr. Adrian Tang from Jet Propulsion Laboratory (JPL). Through the whole designing period, he kept giving me useful suggestions which tends out to be very crucial for the project. I am also grateful to Ph.D student Yan Zhang in High Speed Electronic Laboratory (HSEL) who works closely with me in this project and solve multiple challenging problems in the research. In addition, I would like to thank ChunChen Liu, who provides valuable suggestions to me and innovative ideals in solving the multi-touch detection problems using triangular touch panel pattern in this project. Finally, I am thankful to my all lab-mates who helped me in the test, worked with me in the design and provided me valuable feedback during my presentations.

I would also like to acknowledge all of my colleagues from Qualcomm and Broadcom for helping me during my internships. Many important ideas in this project are originally produced by discussion with them. Besides, I should specially thank to my partners: Yubo Wang and Xuefeng Gu. We came from the same undergraduate school and became close friends, studying and working together in USA for the last five years.

Most important of anything I write here, I have to thank my parents and my girlfriend: Fangting Xia, who constantly support my study at USA. I could not have done it without your selfless love and support.

# VITA

| | |
|---|---|
| January 13, 1989 | Born, Nanjing, China |
| 2007 | B.S., Information Science and Technology, Southeast University, China |
| 2011 | M.S., Electrical Engineering University of California, Los Angeles |
| 2013-2016 | Graduate Student Researcher, University of California. Los Angeles |

# PUBLICATIONS

1. **L. Du**, C. Liu, A. Tang, Y. Zhang, M.-C. F. Chang, "Airtouch: A Novel Single Layer 3D Touch Sensing System for Human/Mobile Device Interactions", ACM/IEEE Design Automation Conference, June, 2016
2. **L. Du**, Y. Zhang, F. Hsiao, A. Tang, Y. Zhao, Y. Li, J. Chen, L. Huang, M.-C. F. Chang, "A 2.3mW 11cm Range Bootstrapped and Correlated Double Sampling (BCDS) 3D Touch Sensor for Mobile Devices", IEEE International Solid-State Circuits Conference, pp. 122-123, Feb. 22-26, 2015
3. **L. Du**, Y. Zhang, C. Liu, A. Tang, Y. Li, M.-C. F. Chang, "A 2.3 mW 11 cm Range Bootstrapped and Correlated Double Sampling 3D Touch Sensing Circuit for Mobile Devices" IEEE Transactions on Circuits and Systems II, April, 2016
4. C. Liu, **L. Du,** Y. Zhang, Y. Li, M.-C. F. Chang, " A single layer 3D Touch Sensing System for Mobile Devices Application" IEEE Transactions on Computer-Aided Design of Integrated Circuits and Systems (Submitted)
5. A. Tang, Y. Kim, **L. Du**, Y. Zhang, F. Hsiao, M-C F. Chang, "Low-Power Chirp-Correlating Spectrometer (CCS) Processor for Deployable Sensor Nodes in 65nm CMOS " , IEEE Transactions on Circuits and Systems II (Submitted)
6. A. Tang, F Hsiao, Y. Kim, **L. Du**, L. Kong, G. Virbila, Y. Kuan, C. Lee, G. Chattopadhyay, N. Chahat, T. Reck, I. Mehdi, M-C F. Chang, "A 95 GHz Centimeter Scale Precision Confined Pathway System-on-Chip Navigation Processor for Autonomous Vehicles in 65nm CMOS", IEEE International Microwave Symposium 2015
7. A.Tang, N. Chahat, Y. Zhao, G. Virbila, C. Lee, F. Hsiao, **L. Du**, Y. Kuan, M. F. Chang, G. Chattopadhyay, I. Mehdi "A 65nm CMOS 140 GHz 27.3 dBm EIRP Transmit Array with Membrane Antenna for Highly Scalable Multi-Chip Phase Arrays", IEEE International Microwave Symposium 2014.
8. Tang, M. C. F. Chang, G. Chattopadhyay, ZZ Chen, T. Reck, H. Schone, Y. Zhao, **L. Du**, D. Murphy, N. Chahat, E. Decrossas and I. Mehdi "CMOS (Sub)-mm-Wave System-on-Chip for Exploration of Deep Space and Outer Planetary Systems" IEEE Custom Integrated Circuit Conference, 2014.

# CHAPTER 1 INTRODUCTION

## 1.1 Motivation

With the development of high performance mobile phones, smart watches, wearable devices, tablets as well as laptops, the human machine interface field became extremely popular. A human interface device (HID) can be regarded as a method that human used to interact with an electronic information system either by inputting data or providing output [1]. Usually, it is an electronic system which tracks the changing property of the users and translates it into certain instructions in the computer, for example, touch sensing, camera based gesture recognition and so on. Among them, one of the most popular HID is touch sensing detection.

Touch sensing, as a general HID, has been widely implemented in various display products (e.g., smartwatches, mobile phones, tablets, laptops and TV). Modern touch sensing systems, which are low power and light weight, created a user-friendly interface for users to control and manipulate electronic devices. As the commercial electronics device become smaller and the required interface experiences are higher, traditional human and machine interfaces such as keyboard typing, mouse clicking are no longer suitable for electronic devices and are all replaced by high-resolution touch interface. According to a recent market report, there will be 2.8 billion touchscreen shipped to the market in 2016 [2]. The popularity of using touch screen in current commercial devices has boosted the touch related research in both academy and industry. Among the reported works, majority of the work are about how to extract accurate finger position on the noisy tight touch space with relative low power consumption [3] [4].

However, among those reported works, the touch sensing technology is still limited to two dimensional (2D) sensing -users are required to touch the screen directly for the system to determine finger position. This technology suffers from various disadvantages, such as fingerprints on the screen or unresponsiveness when hands are wet. Such drawbacks limit the mobile-phone user experience. Beyond these basic limitations, the emerging wearable device market creates additional challenges in touch sensing when compared with traditional mobiles as they offer much smaller display sizes [5], further exacerbating sensing resolution and sensitivity as finger capacitances are reduced.

Problems with current 2D sensing schemes have inspired the development of a remote-sensing solution that will lead to three-dimensional (3D) finger detection. This 3D touch detection system aims at detecting user's finger position remotely and accurately locate user's finger height or gestures in space. Through achieving this, we wish to extend the traditional touch interface experience to another level which provides an advanced human/machine interactions (HMI).

## 1.2 Touchscreen System Structure

A touchscreen system usually contains five components, front panel, touch sensor, touch controller, liquid crystal display as well as system software as shown in Fig.1.1 [6].

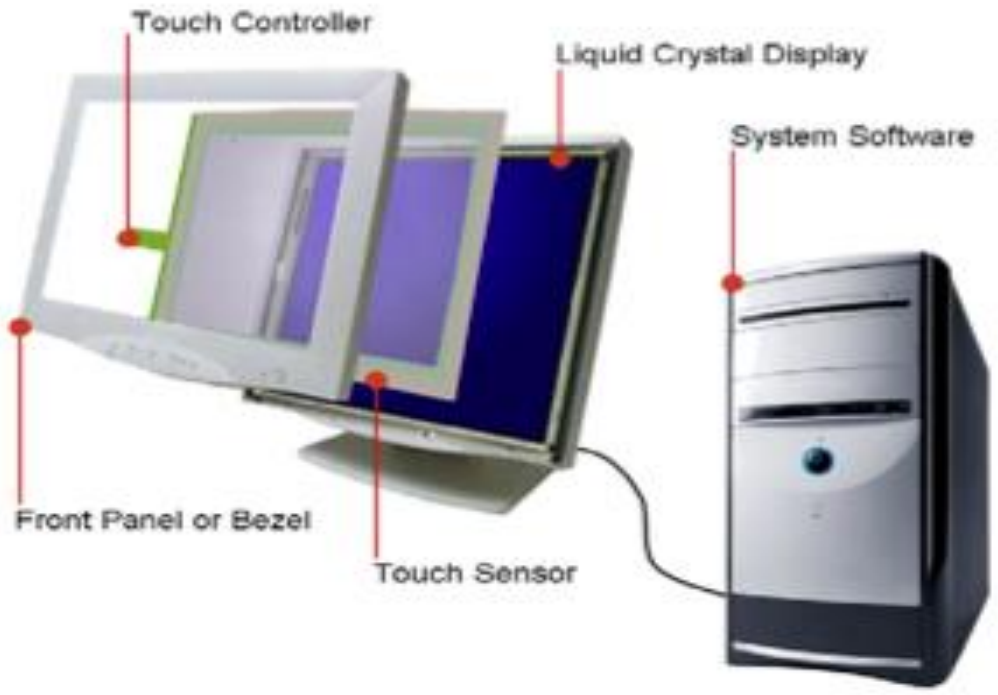


Fig. 1.1 Touch screen system structure

The front panel usually served as a protected shield for touch screen. It stops the outside obstacle such as dust, paper scrap which will affect the touch sensing detection. The touch sensor is usually a glass based panel that has certain response when finger is close or directly touching on the screen. This panel material generally is electrical conducting and depending on the mechanism of sensing, the actual materials used on the cover glass can be different. Most popular technologies for touch sensing nowadays are resistive sensing, capacitance sensing, infrared image based sensing. The detailed implementations of different touch sensing technology will be discussed

later. The touch controller is a system which collects signals from the touch sensor, measures the sensor response and translates it into digital signal that the personal computer (PC) can understand and process. Then the software on the PC side will do post signal-processing to estimate the location of the finger in the screen or understand the customer's instructions. Finally, the liquid crystal display which usually is underneath the cover glass can give feedback to the customer by displaying the request icon or image on the screen [7].

Depending on the application of the touchscreen, these five components can be represented by other electronics devices or combined as one blocks. For example, when touchscreen is used in the mobile phones, the processing engine to estimate finger position is replaced by mobile CPU and liquid crystal display can be replaced by other type of the screen such as LED screen with a smaller size compared to the large display.

## 1.3 Major Work and Organization of thesis

This dissertation is a continuous work of [8]. It begins with reviewing the current development of the touch sensor detection field, and pointing out the trends and benefits to implement 3D touch sensing system which can detect the user's finger motion in space. From that, we introduce the proposed Airtouch Sensing System on Chip (SOC) solutions which includes touch panel pattern design, hardware sensing circuit design and software algorithms to reconstruct finger position. Finally, a mobile-sized prototype system is built and tested in the real-world scenery. Results are analyzed to provide the guidance for future work.

The organization of the thesis is as follows:

Chapter 2 gives a general review of the current popular touch sensor detection technologies in both 2D and 3D. These technologies include resistive touch sensor, capacitive touch sensor, and infrared image based touch sensor. For 3D sensing, we focus on the capacitive sensing technologies and review several reported 3D sensing technologies implementing in large display.

Chapter 3 begins with pointing out the challenges of infusing 3D sensing technologies in smaller display device such as mobile phones or smart watches. Then it presents the detailed implementation of the purposed Airtouch sensing system. Specially, the Chapter 3.2 compares different sensing methodologies that used in existing touch capacitive sensing circuit and conclude that the 3D sensing should use self-capacitive sensing as the sensing methodology instead of the mutual-capacitive sensing. Then in the Chapter 3.3, the proposed triangular touch panel pattern design is introduced. The benefit of using this panel in solving ghost point problems is also explained. Chapter 3.4 introduces the electrical model we built for the touch panel to evaluate the system specification.

Chapter 4 begins to introduce the implementation of the Airtouch hardware sensing circuit. Specifically, Chapter 4.2-4.3 proposes an oscillator based correlated double sampling circuit (CDS) and its relevant calibration technique. Then in Chapter 4.4, the bootstrapping technique is invented to eliminate the inter-channel coupling effect. Next, in Chapter 4.5, an inverter-based LC oscillator is proposed to reduce the chip design cost but providing high-sensitive capacitive sensing. Finally, Chapter 4.6 shows the digital core design and interface design with the PC.

Chapter 5 gives an introduction of the software algorithm used in the Airtouch System. The software algorithm begins with a group filter to remove unexpected channel response. Then the algorithms for each direction's position estimation are explained. EM modelling simulation is included to verify the accuracy of the proposed algorithm to estimate finger position. After that, a reconstructed block is proposed to further remove the system noise effect and smooth the detection.

Chapter 6 reports the Airtouch measurement result and discusses the potential application. The result includes two parts. The 1$^{st}$ part describes the hardware sensing circuit measurement result and the 2$^{nd}$ part reports the system finger position detection resolution. After that, a prototyped platform of the Airtouch system is introduced with a synchronized demonstration video included to demonstrate our system concept. Finally, several potential applications in mobile/wearable devices are discussed.

Chapter 7 draws the conclusion of Airtouch research and gives a direction about further development of this project, specifically it points out that machine learning algorithms can be a potential research direction to improve the sensing accuracy for the 3D touch detection.

# CHAPTER 2 TOUCH SENSING TECHNOLOGY OVERVIEW

## 2.1 Resistive Detection based Touch Sensing

The resistive touch sensor has been very popular during the past ten years. The basic structure of a resistive touch sensor is shown in Fig.2.1. Two layers of transparent resistive material are included in the resistive touch sensor. Generally they are Indium Tin Oxide (ITO) or some other kind of resistive polyester materials. The two layers are placed on top of an insulating layer with a spacer layer to separate each other as shown in Fig.2.1 [9].

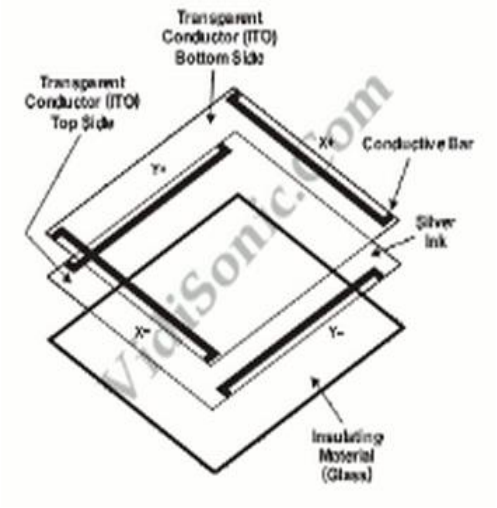


Fig. 2.1 resistive touch screen structure

One of the popular detection methods of this structure is called 4-wire resistive touch sensor and the detection procedure is as explained on Fig.2.2 [10]. Detection is done through first applying a voltage gradient across top layer along the x direction and then measuring the voltage on the other layer. Then applying a voltage gradient across bottom layer along the y direction and

measuring the voltage value on the top layer. When a finger touches the board, it will compress the touch panel (including the spacer layer), in this case the sensor layer works like a voltmeter and can measure the voltage at the touch point through the applied voltage gradient layer. So from the first measurement, we can calculate the touch point along the x direction and for the second measurement, we get the y direction and based on this information, we can calculate the location.

Resistive touchscreen technology works well with almost any stylus-like object, and can also be operated with gloved fingers and bare fingers alike. In some cases, this is more suitable than a capacitive touchscreen, which needs a capacitive pointer, such as a bare finger (though some capacitive sensors can detect gloves and some gloves can work with all capacitive screens). A resistive touchscreen operated with a stylus will generally offer more precise pointing precision than a capacitive touchscreen operated with a finger. Costs are also low when compared with other active touchscreen technologies. However, it is more prone to damage. In addition, the resistive screen's poorer responsiveness to light touches. This has caused it to lose market share to capacitive screens in the 21st century and it became less and less popular in the mobile market now [11].

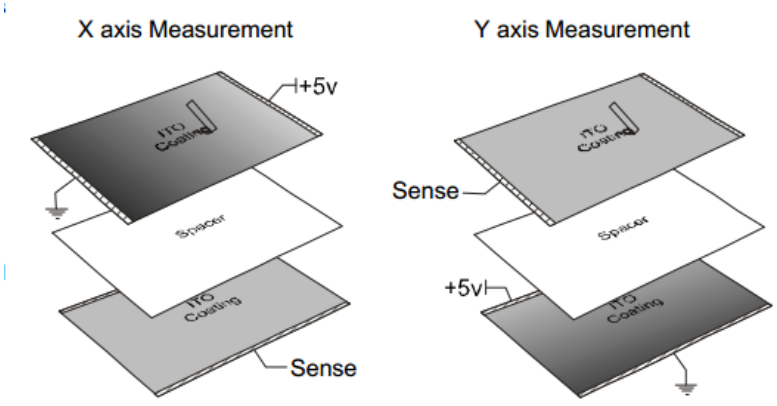


Fig. 2.2 Explanation of resistive based touchscreen detection

## 2.2 Capacitive Detection based Touch Sensing

Capacitance touchscreen usually consist of four multi-layer glasses. The two sides of the glass substrate are covered by conductive ITO and a silicon dioxide hard coating covered on the front side of ITO as shown in Fig 2.3. The working principle can be described as follow [12]:

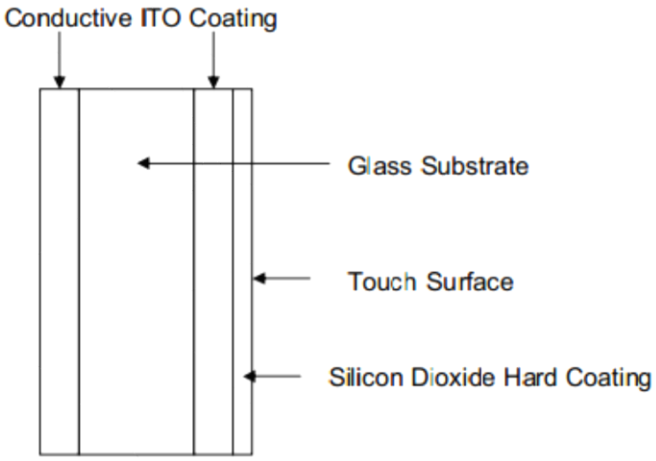


Fig. 2.3 Capacitance based touchscreen structure

Because fingers are conductive, so when a finger touches the screen, it will cause the charge accumulation in the touching area across the glass on the conductive material. Touch screen usually has four sensors on the four corners and measures the amount of charge flowing from each of the sensors to the touched place. Those measured charge information is sent to the touch-controller to calculate the position. One of the typical ways to detect capacitive touch is to apply a voltage on the corner as shown on Fig.2.4, because fingers are connected to ground, so it will attract some current drift to touch point. Theoretically, the total current that drifts from the four electrodes should be proportional to the distance from the touch point to the four corners and based on that it is able to calculate the relative position [13].

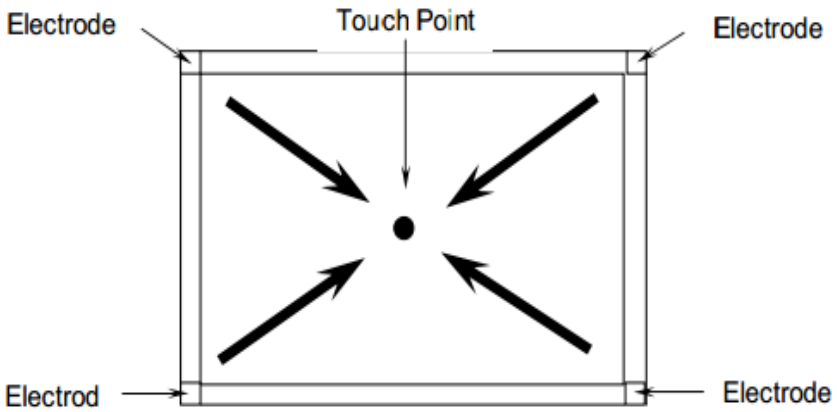


Fig. 2.4 Explanation of Capacitance touchscreen detection

However, the above simple detection can only provide single touch point detection. To provide multi-touch detection, it usually has to be a touch sensor array, for example a 32-by-32 sensor array can provide 1024 points resolution, and voltage can apply to each rows or columns. When fingers are close to the surface of the sensor, it changes the local electrostatic field between row and column channels which affects the mutual capacitance. So by measuring changed capacitance at every individual point on the grid, we can determine the touch location.

These sensor array-type capacitive touchscreen is also called projected capacitive touch technology (PCT). It is a variant of capacitive touch sensing described above. PCT touch screens are made up of a matrix of rows and columns of conductive material, layered on the bottom side of the display glass. This can be fabricated either by etching a single conductive layer to form a grid pattern of electrodes, or by etching two separate perpendicular layers of conductive material to form a grid. The lines are also called electrodes. Voltage applied to this grid will create a electrostatic field, which can be measured. When a conductive object, get close to the PCT panel, it distorts the local electrostatic field at that point. This is measurable as a change in capacitance. If a finger bridges the gap between two of the electrodes, the charge field is further affected. The capacitance can be changed and measured at every individual point on the grid. The more channels,

the better resolutions. Therefore, this system is able to accurately estimate the touch position. Due to the top layer of a PCT being glass, it is a more robust solution than less costly resistive touch technology. Additionally, it is also possible for a PCT system to sense a passive stylus or any grounded objects. There are two types of PCT: mutual-capacitive touch sensing and self-capacitive touch sensing [14].

Fig. 2.5 is a comparison between mutual-capacitive sensing and self-capacitive sensing in the capacitive detection based touchscreen. Unlike self-capacitive sensing, where the sensor directly measured the obsolete change of the finger-to-electrode capacitance change. Mutual-capacitive sensing is measuring the change of the coupling capacitance between two orthogonal electrodes and locating the finger position based on the changed electrodes' cross position.

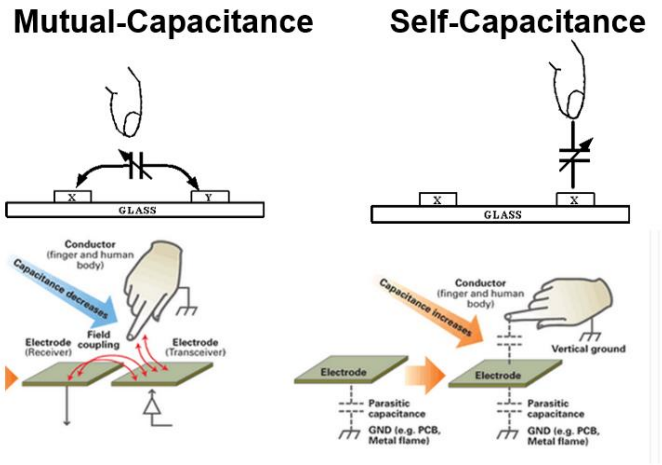


Fig. 2.5 Sensing methodology comparison between self-capacitive sensing and mutual-capacitive sensing

Among these two sensing methodologies in the capacitive detection based touch screen, mutual capacitive sensing become more and more popular. The nature of mutual-capacitive

sensing provides the possibility to support multi-touch detection which self-capacitive sensing cannot support.

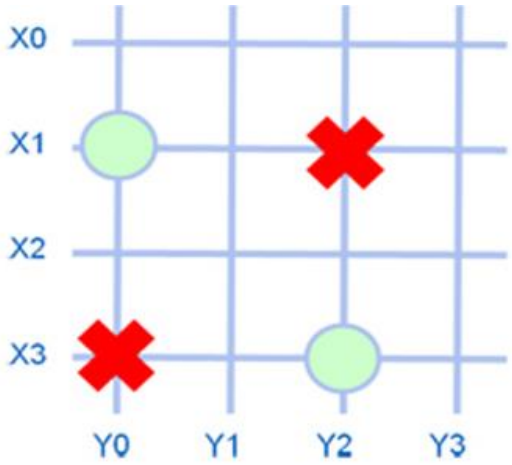


Fig. 2.6 Example of the multi-touch detection in self-capacitive sensing and mutual-capacitive sensing

Fig. 2.6 is an example of the multi-touch detection comparison between self-capacitive sensing and mutual capacitive sensing. The red spots are the place where the touch is happened. The green spots are fake touched place which we will use to compare. If the detection is based on self-capacitive sensing, which measured the electrode's self-capacitive response one by one, the detected changed channel number is X1,X3,Y2,Y0 which is exactly same when you touch on the red spots or on the green spots. On the contrary, if mutual-capacitive detection is employed, the red spots touch will give a response in the mutual capacitance: CX3-Y0 CX1-Y2 while green spots response as CX1-Y0 CX3-Y2.

## 2.3 Infrared Image based Touch Sensing

The infrared image based touch sensor generally uses two infrared transmitters on both sides of the screen which can form a cross-horizontal and vertical infrared matrix. Usually, it is combined with an infrared camera at the bottom of the screen to detect the reflection light from the touch surface. When an object touches the surface, the diffuser under the screen reflects more light compared with in normal case. So if we compare the normal case and the touched case, we will see the reflected signal difference. If we filter out the original reflector signal, we will see additional spots from the camera. Depending on the type of diffuser, it can even detect hover and objects placed on the surface [15]. A typical example is shown in Fig.2.7. When the finger touches the screen, it creates a spot on the camera. This type of the detections works well in both single and multi-touch as shown in Fig.2.8.

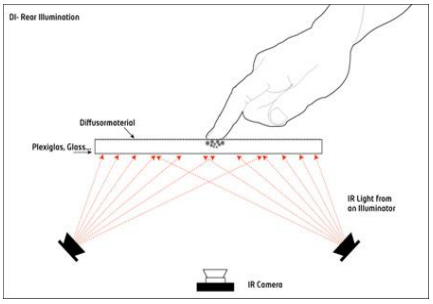


Fig. 2.7 Explanation of Infrared Touchscreen Detection

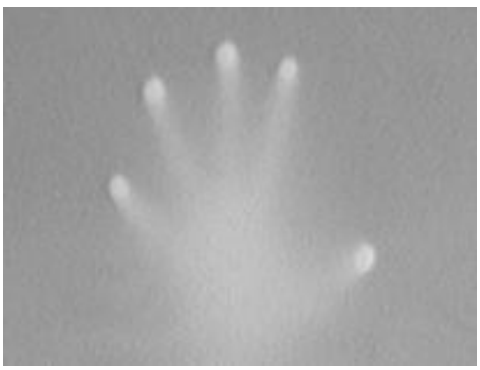

Fig. 2.8 Example of Multi-touch of Infrared Touchscreen Detection

NextWindow, SMART Technologies are companies that dedicated in this technology [16], here we are giving an example of the NextWindow's optical-touch-screen technology. It uses two line-scanning cameras located at adjacent corners of a display as shown in Fig. 2.9.

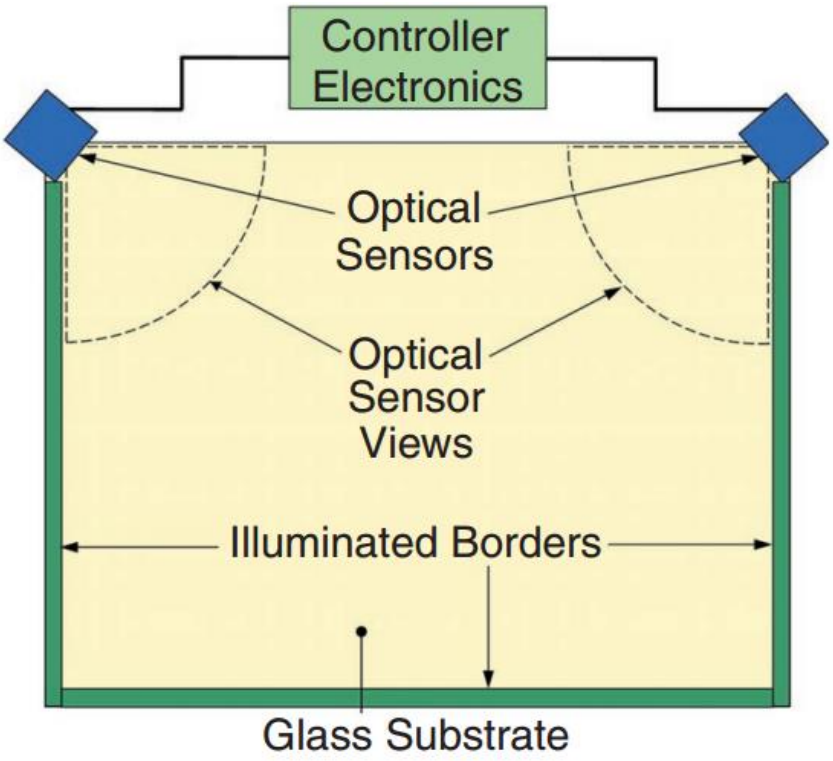


Fig. 2.9 Schematic representation of NextWindow's camera-based touch technology

The camera is used to detect the movement of any object close to the surface by sensing the interruption of the infrared light source. The light is emitted in a plane across the the screen and is reflected back at the cameras by retro-reflecting strips located along three edges of the screen. (Retro-reflectors reflect light back along a path that is parallel to but opposite in direction from the angle of incidence.) When a finger (or any object) touches the screen, the controller gathers the reflected images from the cameras and analyzes triangulates the position of the touching object. These technologies are generally better than other type of the touch screen because they have fewer active components and, therefore, should be lower cost. However, most

applications to date are found on monitor-sized displays or large displays. Although the technology has a sufficiently high resolution and data rate to support handwriting recognition, it is unlikely to be offered for displays below about 10 inch. In this level, the palm rejection is not needed due to border width, and power-consumption concerns. In summary, camera-based optical touch is unlikely to be used in mobile devices in the near future [17].

The disadvantages of the infrared image based touch sensor include the following [18]:

- Accidental activation may occur because infrared beams are actually above the glass surface
- Sensitive to water, snow, and rain
- May be sensitive to ambient light interference
- Higher cost

Those disadvantages limit its application in mobile devices. Specifically, the higher cost of this touch sensor is due to added infrared transmitter and receiver in the mobile devices. Since the mobile devices area is very limited. This additional cost stops its wide implementation in commercial mobile devices.

## 2.4 3D Touch Sensor Technology

Besides traditional touch sensing, recent works in both academy and industry show a trends to extend the touch sensing range from 2D to 3D. This 3D touch, referred as contactless touch detection, aims at detecting the finger position at a certain distance and try to recognize the users' instructions through recognizing the gestures as well as fingers' movement. Several reported works listed below describe their 3D touch technology.

Microchip. Inc in 2013 first proposed a 3D touch sensing detection system as Ref [19]. The architecture of the proposed system is summarized as Fig. 2.10. The system used the TX to send out a low frequency AC signal and use the five RX to receive the capacitance change between the finger and the RX. By detecting the capacitance change between the finger and the five RX, the system reconstruct the finger position in space through comparing those response difference. The algorithm about finger reconstruction through the detected finger capacitance is not listed in any public materials.

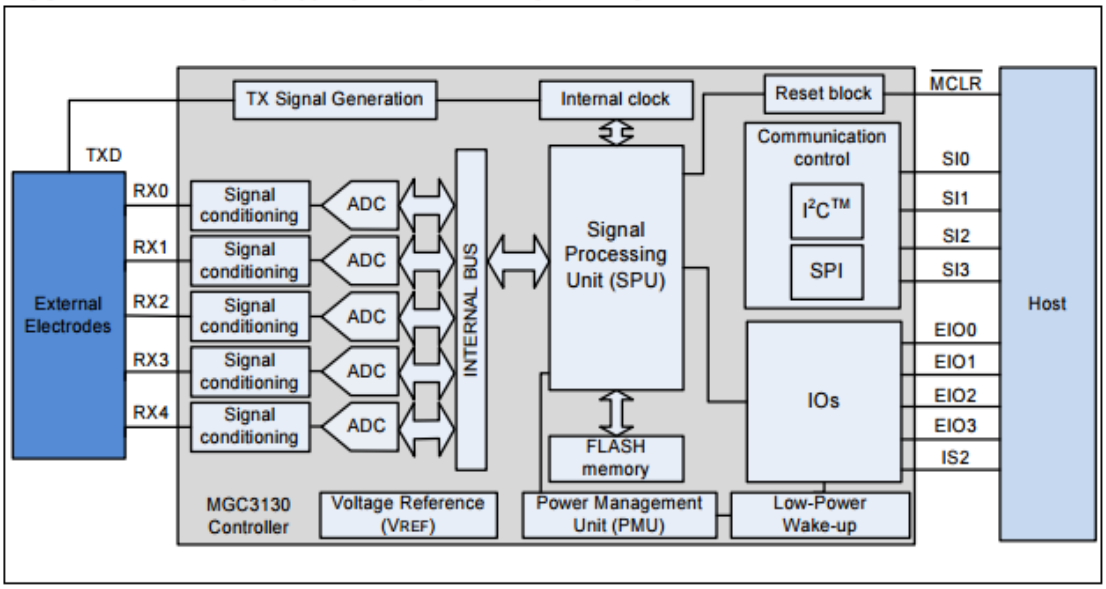


Fig. 2.10 System Diagram of the Microchip MGC3130.

To realize the high-sensitive capacitive sensing, the Microchip is also customizing the touch panel design. The touch panel pattern is shown in Fig. 2.11. According to its reported datasheet, the MGC3130 demonstrates a single-touch detection up to 15cm detection range with a spatial resolution up to 0.17mm and power consumption of 66mW in the acquisition mode.

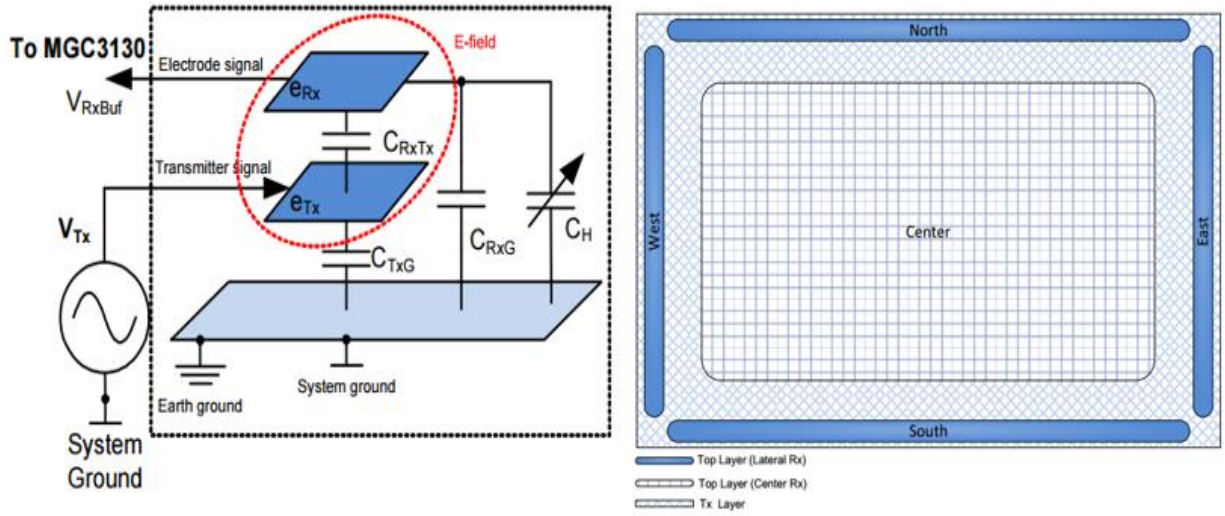


Fig. 2.11 Touch Panel Pattern of the Microchip MGC3130.

In addition to that, Princeton researchers have demonstrated another 3D capacitive touch sensing work in the large display. In their reported work [20], they claimed to use high-Q LC oscillator as the sensing blocks and measure the oscillator load capacitance change to identify the finger-induced capacitance. The system is implemented in a 40cm × 40cm display panel. The electrode-to-electrode distance is 10cm. Fig. 2.12 shows a general system diagram of their proposed 3D touch system.

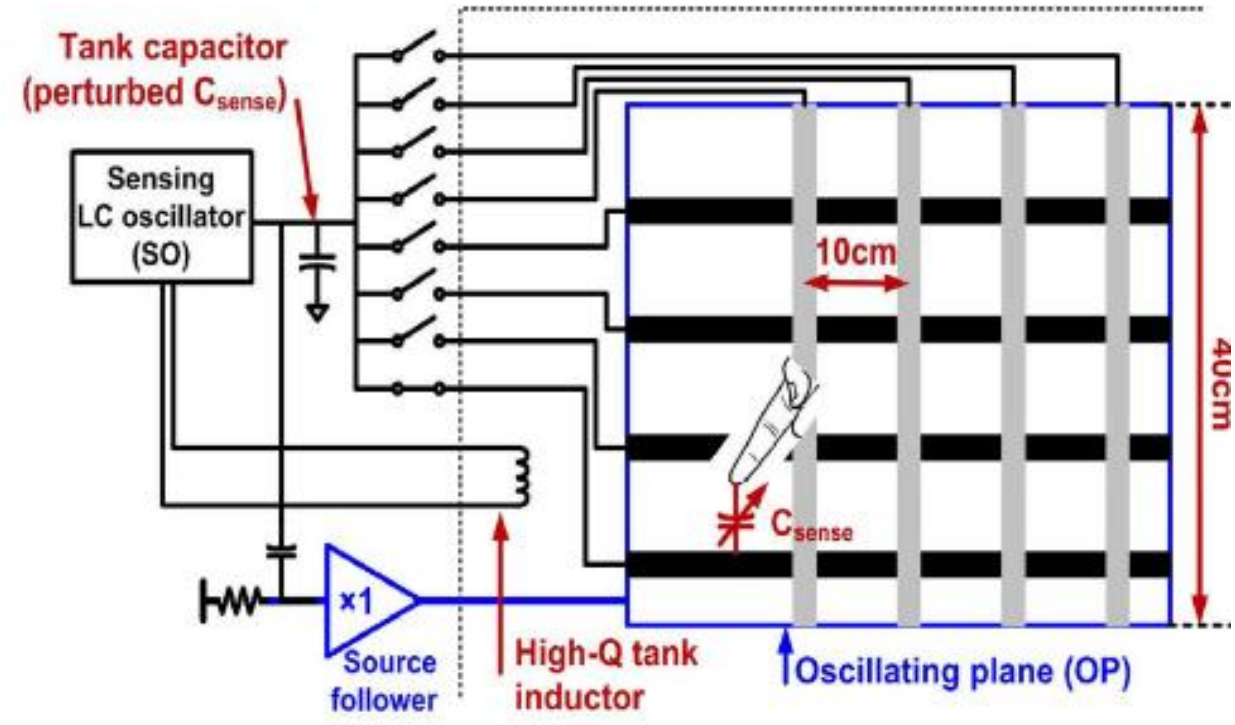


Fig. 2.12 3D Touch sensing system reported in ISSCC by Princeton's researchers.

Based on their paper, this system achieves up to 30cm detection range for hand gesture detection and consumes up to 19mW power consumptions in the acquisition mode. However, no published materials described their software algorithm to reconstruct the finger position in space. In addition, the LC oscillator's frequency is only 200KHz, resulting a high Q off-chip inductor.

## 2.5 Summary of the Reported 2D/3D Touch Sensing Technology

Based on the literature review above, we summarize the following conclusions for the touch sensing technology. For the 2D touch sensor detection, the contact nature provides a short path for the system to sense the user's finger motion, hence the system physical sensing resolution requirement is not high. There are multiple methods used in the industry and academy to achieve high resolution finger position detection in the past ten years. Among them, capacitive touch sensing is the most popular methodology due to its compatibility with nowadays smart phones' screens and the possibility of detecting multi-finger touch.

On the other side, 3D touch sensing is mainly based on the capacitive sensing. The reported 3D sensing works all use two-layer touch electrodes in order to achieve horizontal differentiation and the touch panel size is beyond the regular size of the mobile screens. In addition, the electrode to electrode distance is also more than 10mm which is much larger compared with regular mobile screen electrode distance. Power consumption is also relative high compared with existing 2D touch sensing. Table. I List the typical reported 2D/3D capacitive work specifications.

TABLE I

PERFORMANCE COMPARISON OF THE REPORTED CAPACITIVE TOUCH SENSING WORK

| | ISSCC12 [21] | ISSCC14 [20] | MGC3130 [193] |
|---|---|---|---|
| Sensing Type | 2D Mobile | 3D Large Screen | 3D Large Screen |
| External Component Required | No | Yes(33uH inductor) | No |
| Electrode Spacing | X | 100mm | 48mm |
| Normalized Sensing Height (Height/Panel Area) | 0 | 0.018cm-1 (30cm/(40cm×40cm)) | 0.1cm-1 (15cm/(14.8cm×9.9cm)) |
| Height Resolution | X | 10mm (Screen Size: 40cm×40cm) | X |
| SNR | 35dB@0cm | 50dB@5cm 30dB@16cm | X |
| Power Consumption | 10.6mW | 19mW | 66mW |
| Die Area | 6.87mm$^2$ | 4.2mm$^2$ | X |
| Technology | 1.5/5.5/30V 90nmLDI | 1.2/2.5V 130nm CMOS | X |

# CHAPTER 3 AIRTOUCH SYSTEM OVERVIEW

## 3.1 Challenges of Implementing Mobile 3D sensing

As described in above Chapter, to implement the 3D touch sensing in the mobile devices, there are several challenges need to overcome.

The 1st challenge is the sensed active finger capacitance is dramatically reduced compared to the 2D sensing where the finger is touched on the screen. This makes the touch system sensitivity requirement to be much tighter. To accurately evaluate the sensed finger capacitance change, we have built an EM model to verify the finger induced-capacitance versus its height (vertical distance between the finger and the touch plane). The result is shown in Fig. 3.1. When the finger height is above 5cm, the finger induced capacitance is less than 50fF.

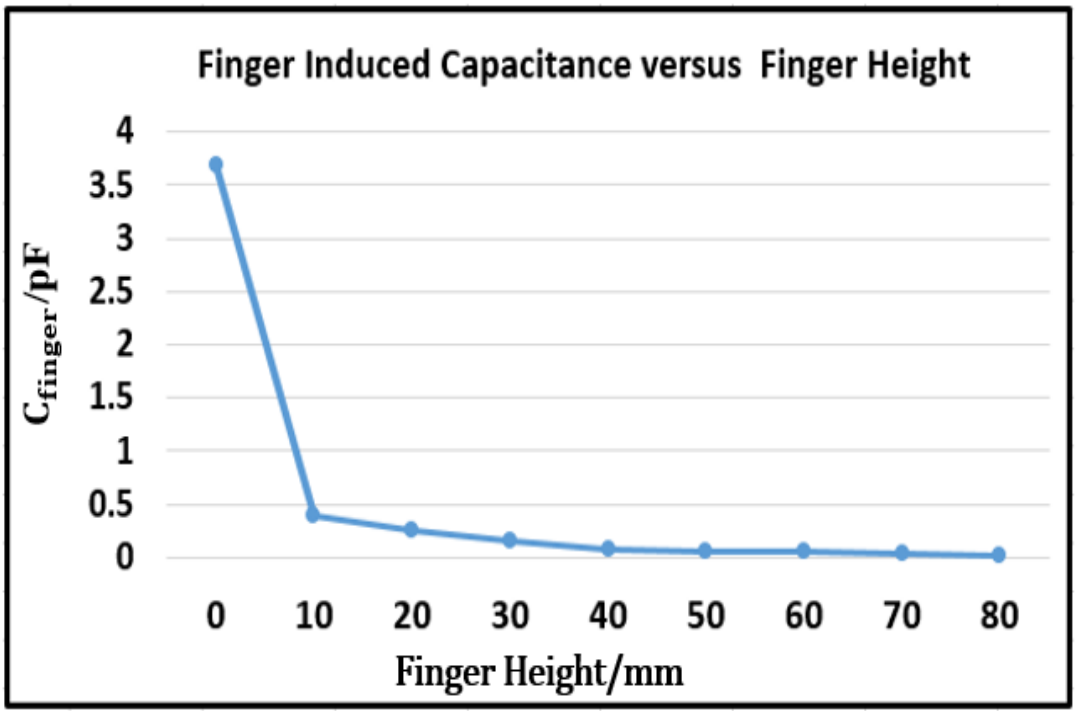


Fig. 3.1 Finger induced-capacitance versus its height

In additional to the 1st challenge, the 2nd challenge to implement 3D sensing on mobile screen is about how to eliminate large channel-coupling effects. Unlike touch screen in large display that reported in Chapter 2.5, touch screen in mobile devices is not allowed to be customized with large electrode distance which obviously will reduce the 2D sensing resolution dramatically. To implement 3D touch sensing in mobile devices, we need to rely on the existing 2D sensing touch panel used in the mobile device market, tolerating a tight electrode-to-electrode spacing. This physical nature causes a large inter-channel coupling effect which needs to solve. Regular touchscreens in the market are usually two-layers with one layer electrodes in the horizontal directions and the other layer's electrodes are in the vertical directions. Large coupling is shown between these orthogonal channels due to the tight space between these two.

Fig. 3.2 is a typical structure of the touchscreen used in the market. The touchscreen has two-layer electrodes, both layers' electrodes are diamond-shaped. The corresponding electrical model is shown on Fig. 3.3.

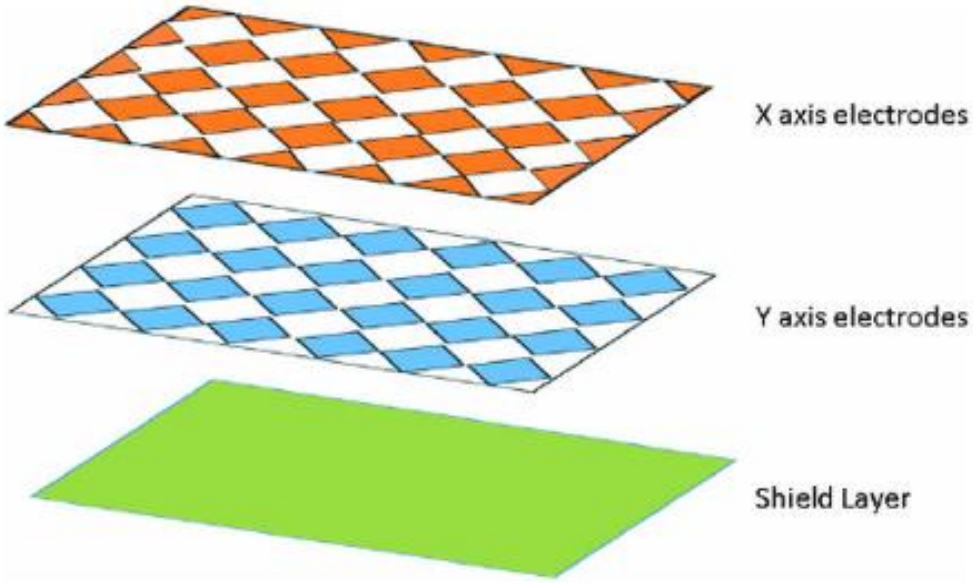


Fig. 3.2 Diamond shape touch screen architecture

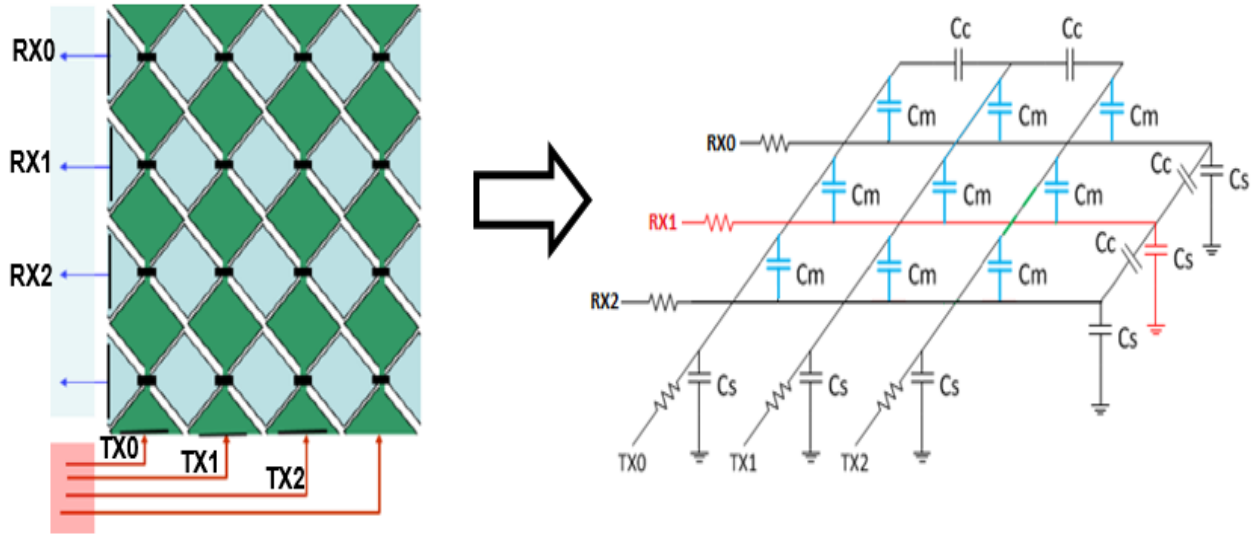


Fig. 3.3 Diamond shape touch screen's electrical model

## 3.2 General Sensing Approach Comparison

As described in Chapter 2.5. Among those reported 3D sensing works, employing large electrodes on the display is a common approach. Through this, the system mitigate the electrodes' coupling effects of the touch panel and increase the sensed finger capacitance. However, this approach not only requires a large-sized touch panel but also consumes large power consumption due to the large electrode size, making it not possible for the mobile device where the screen size and power is limited and electrode deposition cost is expensive.

To implement 3D touch sensing technology into volume and power-constrained mobile devices with low cost, we need to find a suitable capacitive sensing approach. The current 2D capacitive touch sensing can be mainly categories as the self-capacitive sensing and mutual-capacitive sensing as described before. Although the parasitic mutual capacitance of the touch electrode is generally much larger than the self-capacitance, mutual capacitive sensing is still widely used as the main 2D touch sensing methodology in the mobile industry due to its compatibility of implementing multi-touch detection. For self-capacitive sensing, multi-touch detection cannot be supported due to the potential generation of ghost point during the electrode scanning shown as Fig. 3.4 [22]. For example, the touch screen is touched with two fingers that are diagonally separated and detected through self-capacitive sensing, a pair of "ghost points" are created because the controller only knows that two columns and two rows have been touched; it cannot tell which coordinate pairs belong.

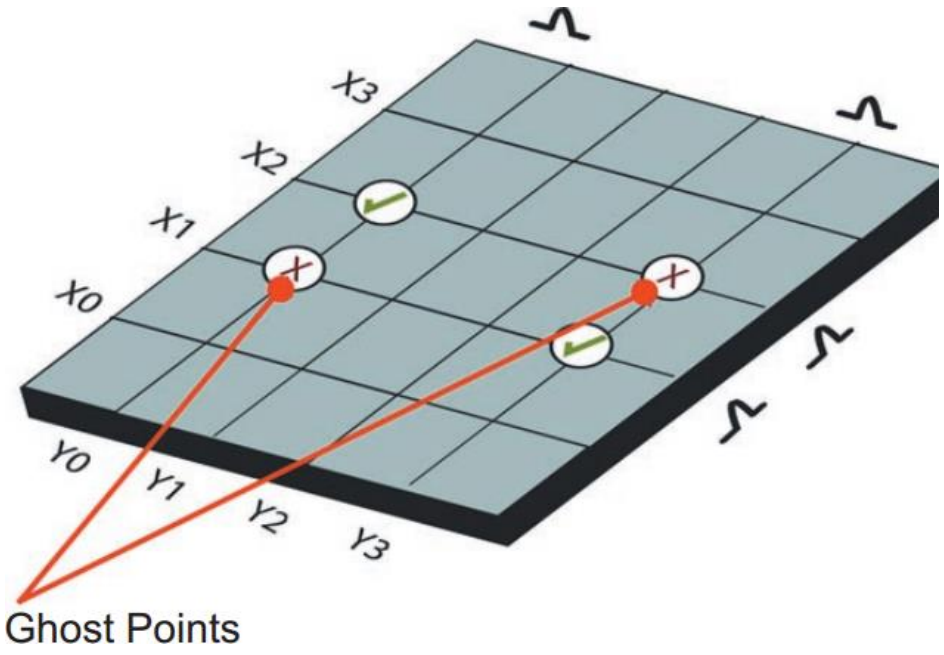


Fig. 3.4 The touch screen is touched with two fingers that are diagonally separated

Although the mutual capacitive sensing avoids the generation of the ghost points, it also creates a large parasitic coupling capacitance. Through experiment, we have seen around 60pF coupling capacitance between channels to channels in the HTC Cesar mobile screen [23]. On the other hand, the electrode's intrinsic self-capacitance is around 500fF. In normal 2D contact detection, the finger-induced capacitance can be as large as 20pF, reducing the parasitic capacitance requirement.

Besides, compared with 2D touch sensing, the contactless nature of the 3D touch sensing has created an air gap between the finger and the thin touch glass. This requires the touch panel's electrode to sense a much smaller finger capacitance [24]. If using mutual-capacitance sensing as the sensing approach, we need to detect a femto farad level capacitance change in a fixed parasitic

capacitance at 60pF level. On the contrary, if using self-capacitance sensing, the system needs to detect femto farad level capacitance change with a parasitic capacitance around 500fF.

To maximum the system sensitivity, the self-capacitive sensing becomes the best approach for 3D touch detection. However, this cause another problems that the self-capacitive sensing cannot support multi-touch position detection, resulting a limited user-experience. In the following chapter, we will introduce our single-layer touch panel pattern design to enable multi-touch detection while using self-capacitive sensing.

## 3.3 Single-Layer Touch Panel Design

As described above, one of the drawbacks for the common two-layer touch panel is that it is unable to detect multi-finger position through self-capacitive sensing. On the other side, the 3D touch sensing approach can only be self-capacitive sensing due to the reduction of the active finger capacitance. Besides, the design cost of a two-layer touch panel is much higher than single-layer touch panel.

To solve this pair of conflicts and also reduce the manufactory cost, we have proposed a single-layer touch panel pattern design that can support multi-touch detection through self-capacitance sensing and aim at reducing the fabrication cost by half through using only one-layer electrodes. The sensing electrodes have been designed as triangle shapes as opposed to the normal diamond shapes. This provides a Y direction detection ability through calculating the upper channels' and lower channels' detected finger-capacitance ratio. This touch panel pattern is first proposed in the 2D touch sensing application by Dr. Chunchen Liu in HSEL [25]. In this project, we have implemented similar design for the 3D touch sensing.

Moreover, this structure also avoids the generation of diagonally ghost points which limits the traditional self-capacitive touch sensing to multi-touch detection. The triangle shaped electrode may create an ambiguity regarding of the multi-fingers' position if the fingers are exactly aligned together in the same X direction, however, this is a recoverable position error as opposed to the totally different diagonal ghost points happened in the normal two-layer touch panel. Fig. 3.5 gives an example of this type of the touch panel with six channels. However, the real number of the channels can be changed depending on the applications and hardware availability.

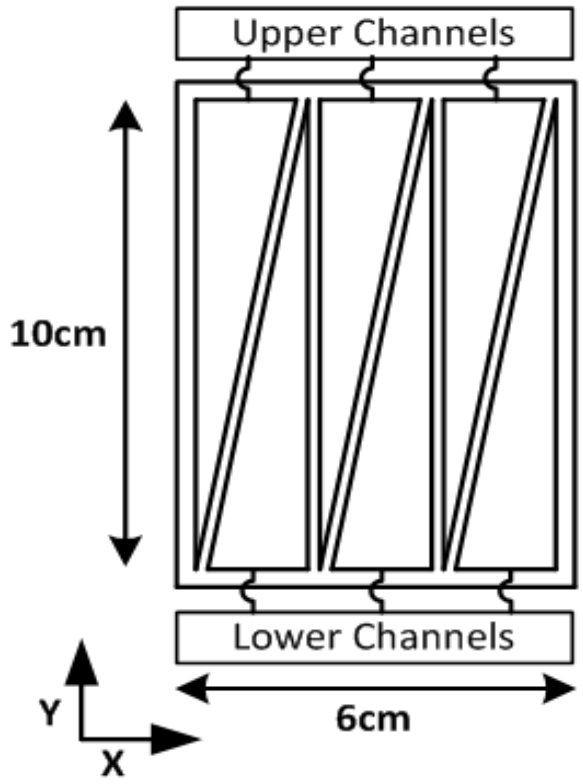


Fig. 3.5 Example of the triangle shaped single-layer touch panel design

To accurately model the performance of this proposed architecture, we have put the touch panel pattern in the Ansoft Q3D EM Software. We build the finger model as a grounded-10cm-height cylinder and measure the finger to channel's capacitance at different Y position in different finger height shown as Fig. 3.6. The simulated results are summarized in Fig. 3.7. The designed size of the electrode senses a finger induced capacitance response of more than 40fF up to 5cm finger height which is large enough for analog circuitry to detect [26]. Moreover, the sweep of the finger Y direction at the same height shows a comparable difference in the electrode's self-capacitance. This illustrates that it is sufficient for the system to determine the Y position by comparing two nearby electrodes' self-capacitance.

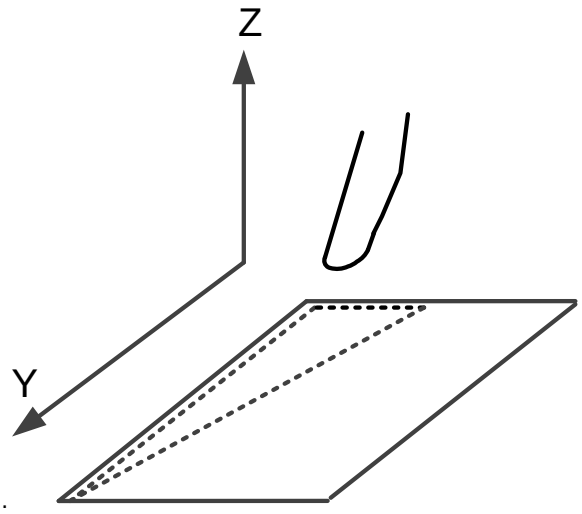


Fig. 3.6 EM modelling touch panel with the finger movement in the space

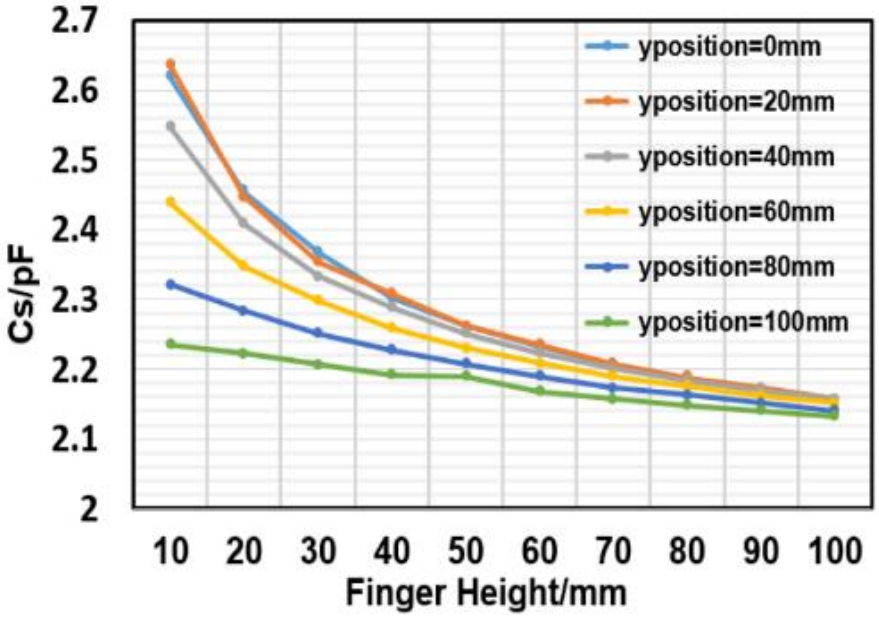


Fig. 3.7 Simulated Finger Height versus channel self-capacitance response

## 3.4 Touch Panel Modelling

In additional to the touch panel pattern design, the suitable electrical modelling of the touch panel also plays an important role in defining hardware circuit specifications and evaluating the system performance. The electrodes of the touch panel are usually fabricated through depositing ITO on the screen with a sheet resistance between 10-100 ohm/square [27]. This large sheet resistance provides a routing resistance that cannot be ignored in the touch panel modelling. Besides, each touch electrode will have a self-capacitance to the ground and mutual capacitance to its nearby electrodes. The self-to-ground capacitance serves as an additional load for the detection circuit so as reduce the system sensitivity and the mutual capacitance creates a shorting path from electrodes to electrodes, limiting the accuracy of finger position estimation.

In order to accurately model each parameter's effect on the system performance, the long electrode is deposited into several portions, providing an RC constant of each portion to be much smaller than the sensing signal's periods. Fig. 3.8 shows an example of depositing the electrode into three discrete lumped RC units. In each unit, $C_s$ represents the electrode's self-capacitance of that particular portion, while $C_m$ represents the coupling capacitance to its nearby parallel electrode. The $C_s$ and $C_m$ can be obtained through an EM simulation while the R can be calculated based on the analytical expression below:

$$R = R_s \times \frac{2L}{3}(W_u + W_d) \quad (1)$$

Where the $R_s$ is the sheet resistance of the ITO, L is the length of the electrode on Y direction, and $W_u$, $W_d$ correspond to the upper and lower width of the electrode's on X direction's in each portion. In the following section, we will describe the hardware self-capacitive sensing circuit implemented in the Airtouch system.

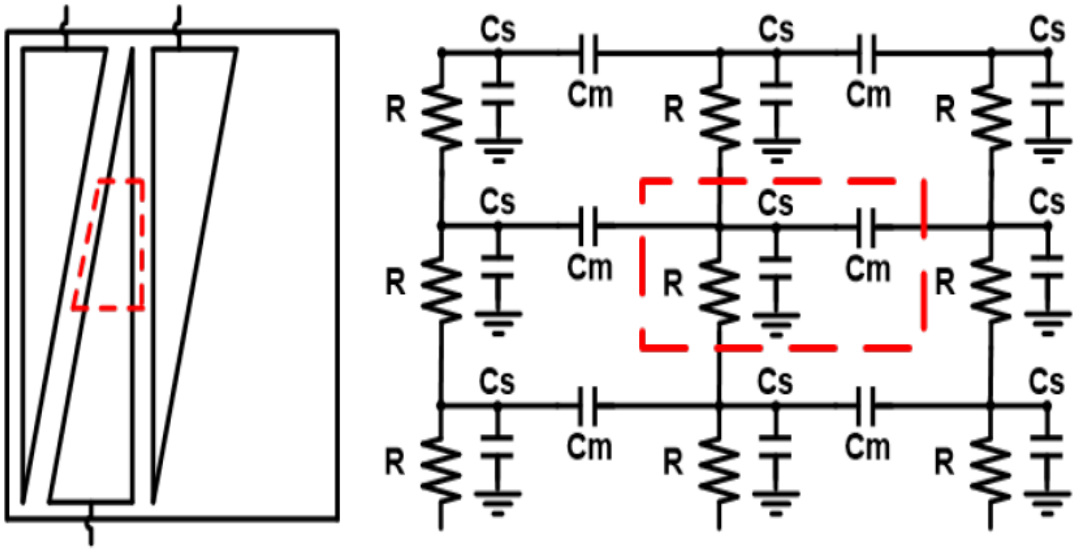


Fig. 3.8 Modelling of the touch electrode with one unit portion highlighted

# CHAPTER 4 AIRTOUCH HARDWARE SYSTEM

## 4.1 Hardware System Architecture

The hardware sensing system design is explained in this chapter. The system contains three major techniques to solve the 3D sensing challenges described in Chapter 3.

1. An oscillator-based CDS module with trimming capacitor array at the oscillator input to enable high resolution self-capacitance sensing.
2. A bootstrapping circuitry to mitigate the inter-channel coupling effects, providing horizontal direction differentiations.
3. An on-chip inductor-less resonator as the capacitive sensing blocks to reduce production cost.

Fig. 4.1 gives an overview architecture of the hardware sensing system with major blocks highlighted.

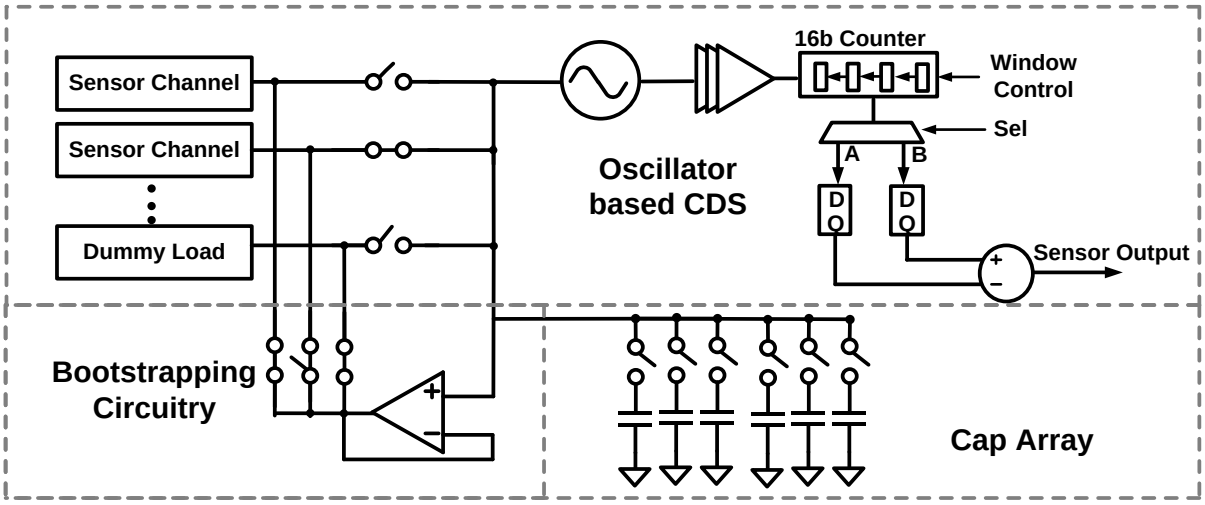


Fig. 4.1 Overall of the Airtouch Hardware System Architecture

## 4.2 Oscillator-based CDS

The channel's load capacitance change is measured through an inverter-based LC oscillator whose frequency is monitored via a digital counter with a specific integration time (observing time window). Unlike traditional oscillator-based capacitive sensing, the integrated counter value will be directly equated with the channel's load capacitance. The CDS sensing uses a dummy load to cancel the channel's intrinsic self-capacitance and only outputs the sensed finger-induced capacitance of the channel. During each measurement cycle, the oscillator is first connected to the desired input sensor channel for a given integration time and then connected to a dummy load with similar capacitance for the same integration time. During each integration window, a digital counter records the number of periods that the oscillator completes which reflects the oscillation frequency. Fig. 4.2 shows the overall oscillator based CDS block diagram.

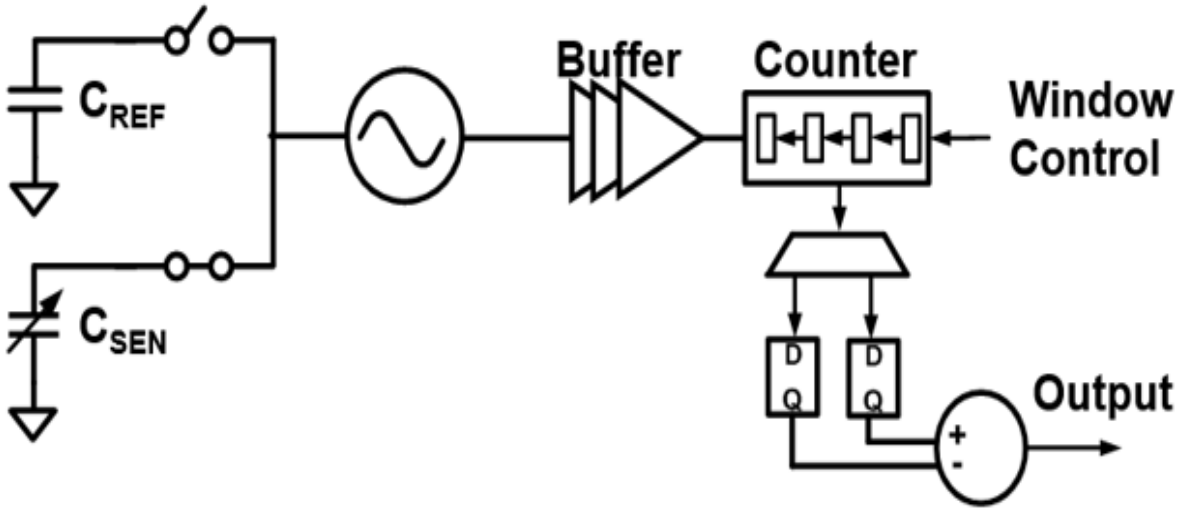


Fig. 4.2 Overall Oscillator based CDS sensing architecture

The sensing procedure is as follows: In the 1st cycle, the oscillator connected to the sensor channel, and measure the oscillator frequency: $f_{sen}$. Then, the oscillator is connected to the reference channel (dummy channel) and the counter measures the oscillator frequency: $f_{ref}$. Finally, the system output the minus of these two measured frequency ($f_{sen} - f_{ref}$) as the final output.

Since the finger-induced capacitance is very small compared with the channel intrinsic self-capacitance, the output counter code difference is directly proportional to the sensed finger capacitance derived as (2).

$$C_{finger} = \Delta C = \frac{1}{4\pi^2(f-\Delta f)^2 L} - \frac{1}{4\pi^2 f^2 L} \approx \frac{\Delta f}{2\pi^2 f^3 L} \tag{2}$$

Where $f$ corresponds to the oscillation frequency and $L$ is the oscillator's inductor value. In addition, if the active channel's intrinsic capacitance and dummy channel load are well matched, any low frequency noise (i.e Oscillator's flicker noise) will be shown in the counter value of both the active channel case and the dummy channel case. By outputting the counter's difference between the input channel and dummy channel, the system will cancel most of the low frequency noise through generating a zero at the DC in its frequency transfer function. The equivalent frequency transfer function of the CDS integration can be derived as (3) and (4).

$$Y(t) = \int_{t-t_0}^{t} X(t) - \int_{t}^{t+t_0} X(t)$$

$$= \int_{-\infty}^{t} 2X(t) - X(t-t_0) - X(t+t_0) \tag{3}$$

$$H(f) = \frac{F(Y(t))}{F(X(t))} = \frac{1}{j2\pi f}\left(2 - e^{j2\pi t_0 f} - e^{-j2\pi t_0 f}\right)$$

$$= \frac{4\sin(\pi t_0 f)^2}{j2\pi f} = -2jsinc(\pi t_0 f) t_0 \sin(\pi t_0 f) \tag{4}$$

Where t0 is the integration window time. When $f$ is close to DC, the transfer function can be approximated as (5), showing a zero at the DC.

$$H(f) = -2\pi j sinc(\pi t_0 f) {t_0}^2 f \tag{5}$$

In (6) (7), we derive the transfer function for a system without correlated sampling, showing low-frequency noise exhibits a large gain near DC, limiting the system's sensitivity to small changes of capacitance. Fig. 4.3 shows the comparison between CDS transfer functions and non-CDS transfer functions. As it shows, the CDS transfer functions provide a large noise attenuation at low frequency, resulting a highly sensitive capacitive sensing system.

$$Y(t) = \int_{t-t_0}^{t} X(t) = \int_{-\infty}^{t} X(t) - X(t - t_0) \tag{6}$$

$$H(f) = \frac{F\big(Y(t)\big)}{F\big(X(t)\big)} = \frac{1}{j2\pi f}\left(1 - e^{-j2\pi f t_0}\right)$$

$$= sinc(\pi t_0 f) t_0 e^{-j\pi f t_0} \tag{7}$$

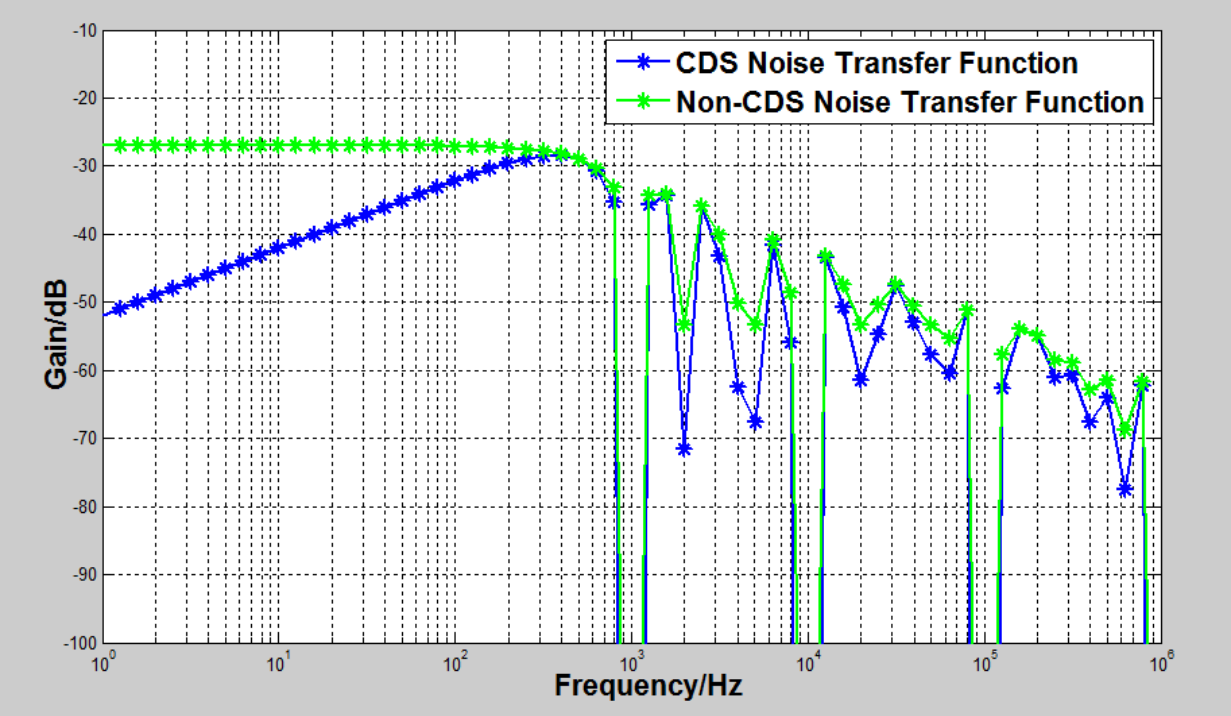


Fig. 4.3 Noise Transfer Function Comparison between CDS and Non-CDS architecture

Through Fig.4.3, we see around 20dB attenuation of the low frequency noise between CDS and Non-CDS. However, in order to provide CDS function, the reference channel should have same load properties as the active ones. In this case, the two measurement results are correlated. In addition, all the sensing channels should also have same load properties. Thus, the ratio between the frequency shift and the measured finger capacitor value for each channel are same. The measured frequency shift can be represented as the detected unified finger capacitance.

To trim all the channels to have equal load properties, a two-step calibration algorithm is introduced in the following sections.

## 4.3 Calibration of the Channel Load

As discussed in Chapter 4.2, in order to use the CDS to cancel noise, an equal electrical load capacitance among all channels including the dummy channel is necessary. To achieve this, a two-steps channel load trimming calibration scheme is employed. Fig. 4.4 shows the 1st step of the calibration sequence which searches for the maximum-load-capacitance channel. The system scans each channel and monitors the counter value (equated to oscillator frequency) for a fixed time. In each scan, the counter's output result stored in RegA will be compared with the RegB's value. If it is smaller than the RegB's value, it will replace the current RegB's value. After the scanning, the maximum channel's load capacitance value will be stored in RegB as the reference load value which is used to calibrate the remaining channels' load capacitance.

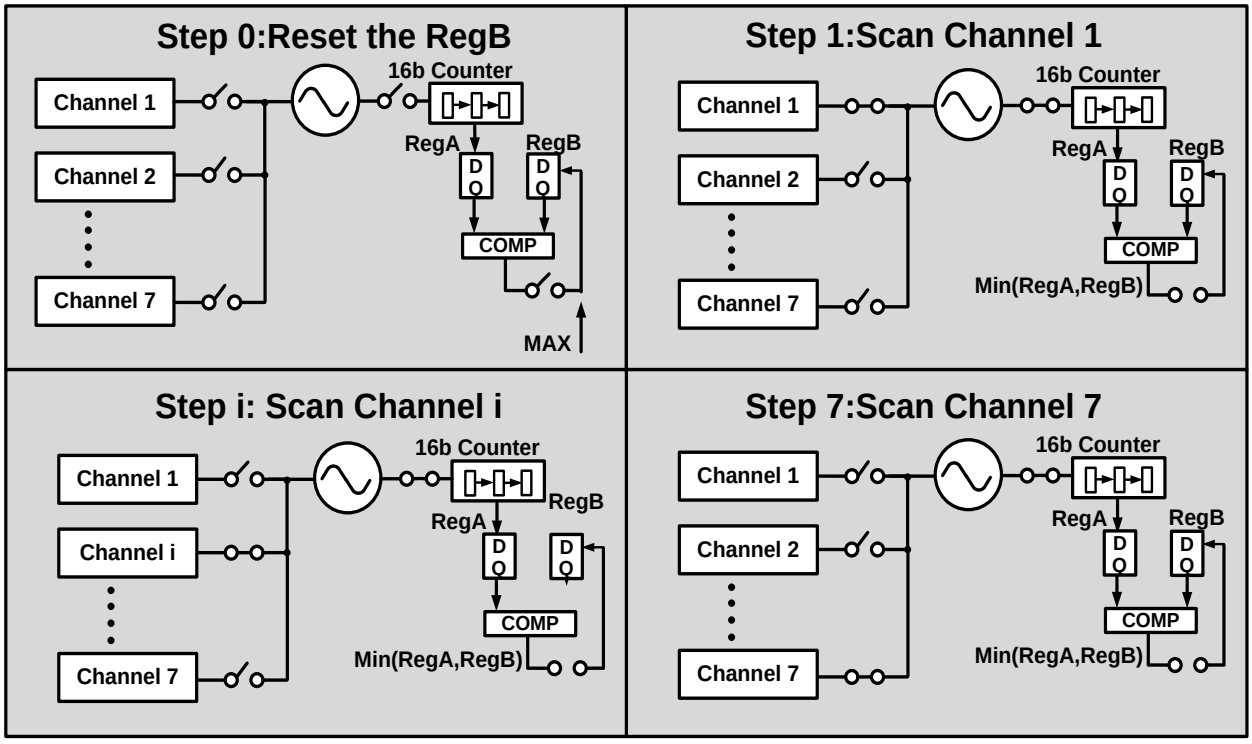


Fig. 4.4 Procedure for determining the maximum channel load

During the 2nd step of the calibration, each channel will be calibrated individually by using a switched capacitor array to trim the channel capacitance to closely match the reference load value. This is achieved by successively approximating the readout counter value to be as close as the RegB's value through a 6-bit binary capacitor array as shown in Fig. 4.5. After the calibration sequence, the capacitor array's value will be stored in the memory and will be loaded during normal scanning to trim each channel's load to match the reference. In normal scanning, if no finger is approaching the sensor, the CDS output will remain close to zero, while if a finger is approaching, the counter will output a positive number.

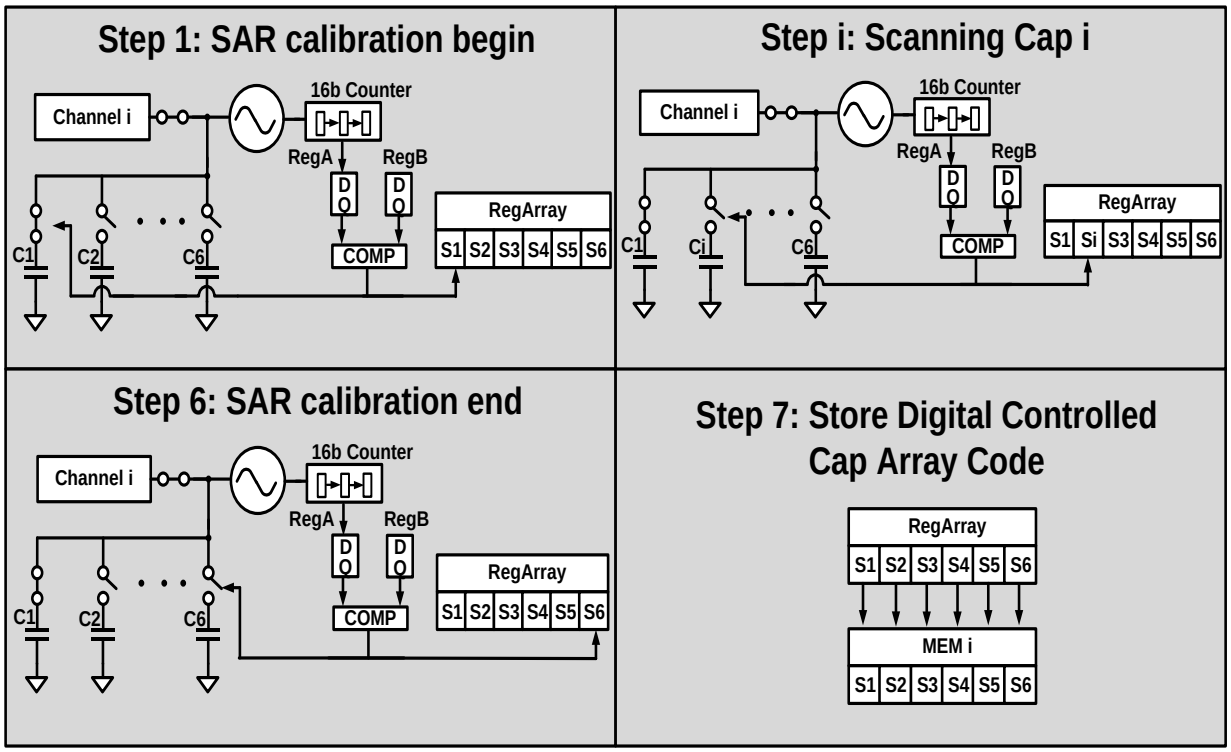


Fig. 4.5 Procedure of calibrating Channel I's load using a SAR algorithm

The state machine diagram for this calibration is described in Fig. 4.6. The calibration as described before is using SAR operations. The whole calibration begins only one time during the

power up. The calibration algorithm is currently implemented through the software side as the circuit only required one time calibration. The control of each digital trimming capacitor is through the digital core block which connected with the PC through USART. The following chapters will describe the details about this interface.

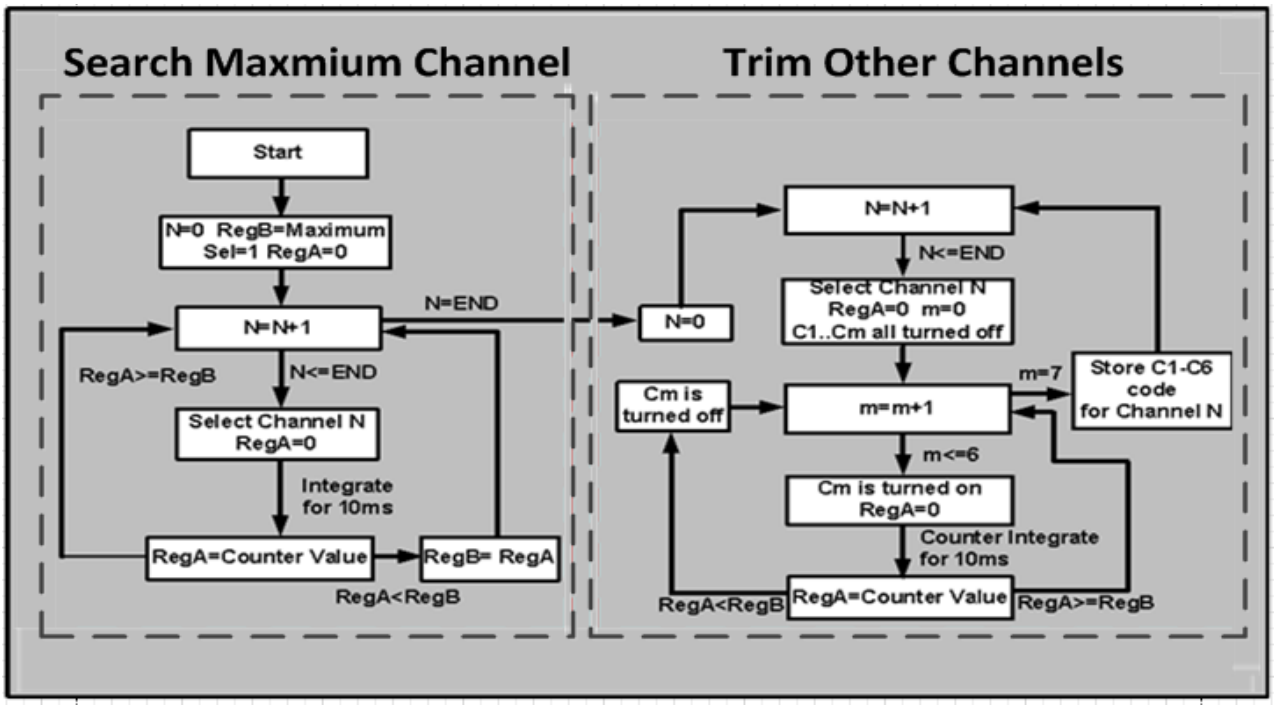


Fig. 4.6 State machine diagram of the channel-load calibration

## 4.4 Bootstrapping Technique

In addition to the challenges of detecting the small finger capacitance change in 3D sensing compared with 2D sensing, the large channel-to-channel coupling capacitance (typically in the range of 20pF-100pF for a mobile screen) also limits the system sensitivity, causing a resolution degradation in the horizontal direction during the channel scanning process. This difficulty is illustrated in Fig. 4.7.

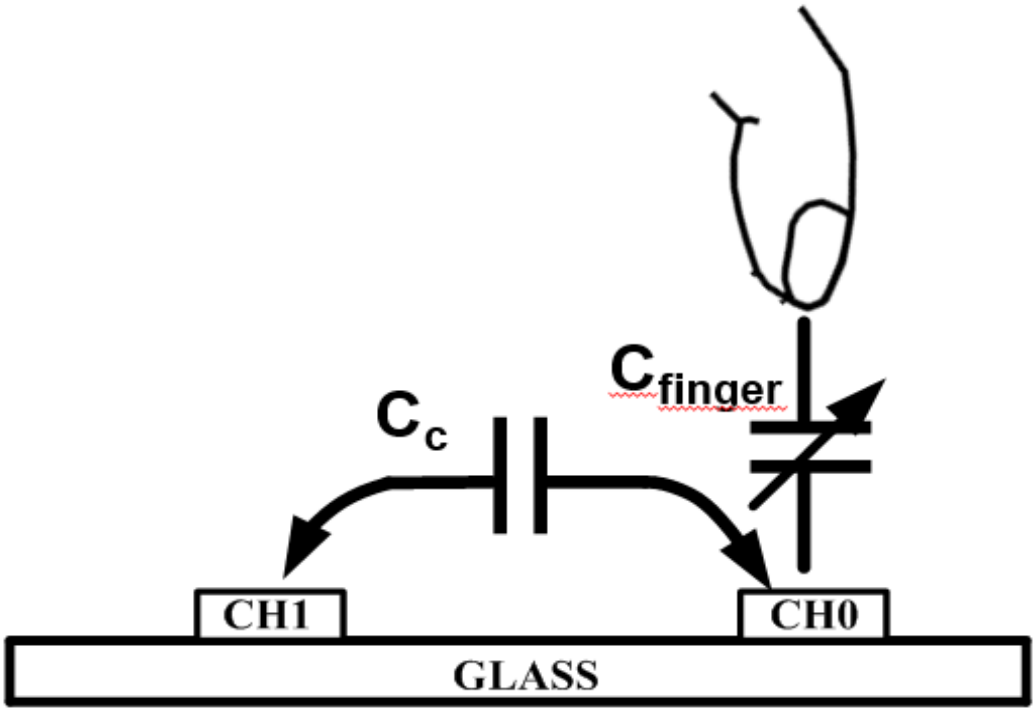


Fig. 4.7 Channel coupling effect in small touchscreens

(when $C_c$>> $C_{finger}$, both CH0 and CH1 will show an equal response)

When the finger is approaching Channel 0 (CH0), a femto-farad level finger capacitance $C_{finger}$ is induced onto CH0. Ideally, the system should only see the induced capacitance experienced as an increase in CH0's self-capacitance. However, if the inter-channel capacitor $C_c$

is much larger than $C_{finger}$, the finger capacitance will couple to CH1 through $C_c$, providing an equal channel response among CH0 and CH1, which will cause a false horizontal position detection. To overcome this, bootstrapping circuitry is introduced between channels to eliminate the coupling capacitance as depicted in Fig. 4.8. As the electrodes array is scanned, a unity-gain amplifier is used to sense the time-domain voltage of the currently active channel and replicate it on the remaining inactive channels to nullify the coupling capacitance by enforcing equal potential across the inter-channel coupling capacitors. In this case, the coupling capacitance seen from the active channel is suppressed.

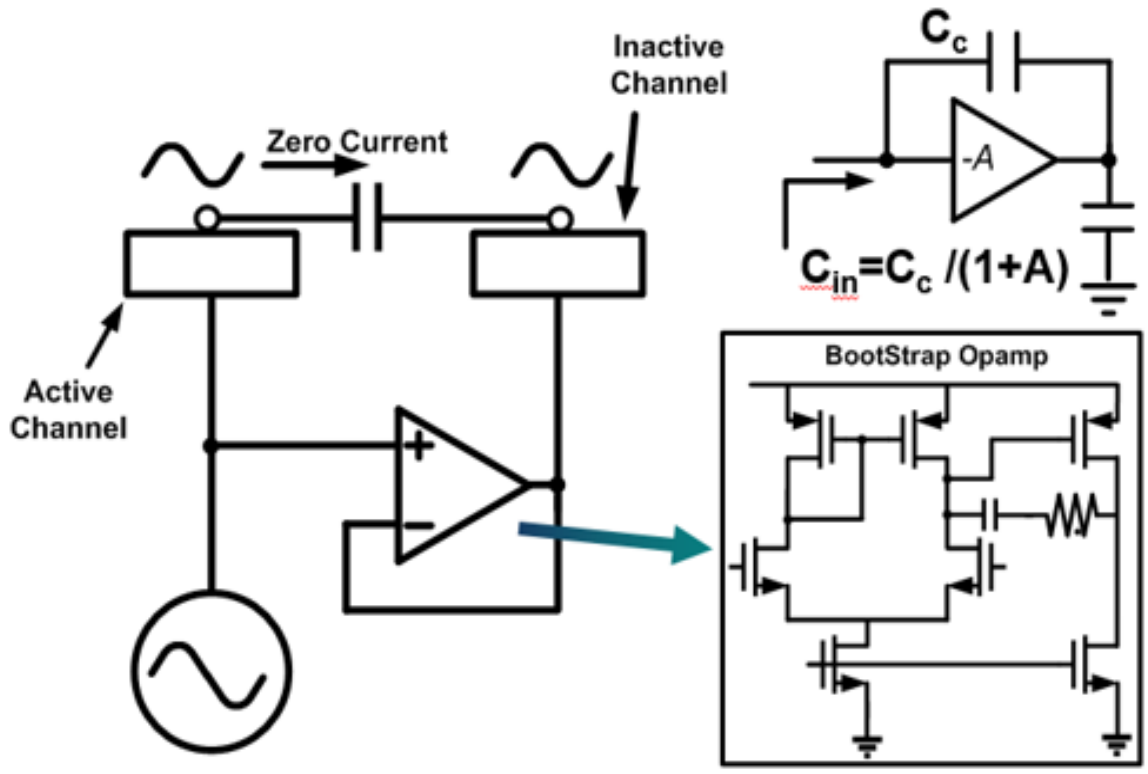


Fig. 4.8 Introduced bootstrapped circuitry showing the suppression of the coupling capacitance through the tracking amplifier.

The derivation of the bootstrapping technique is as (8) (9). The corresponding circuit model is shown in Fig. 4.8.

$$Vout = \frac{A}{A+1} Vin \tag{8}$$

$$Zin(s) = \frac{Vin}{Iin} = \frac{Vin}{(Vin-Vout)sCc} = \frac{Vin}{\frac{sCc}{(A+1)Vin}} = \frac{A+1}{sCc} \tag{9}$$

As it shows in the equation, the input capacitance looking from the active channel is reduced to 1/(A+1) of the coupling capacitance as before. To achieve enough suppression, a gain of 45dB two stage amplifier is designed to lock the idle channels' voltage.

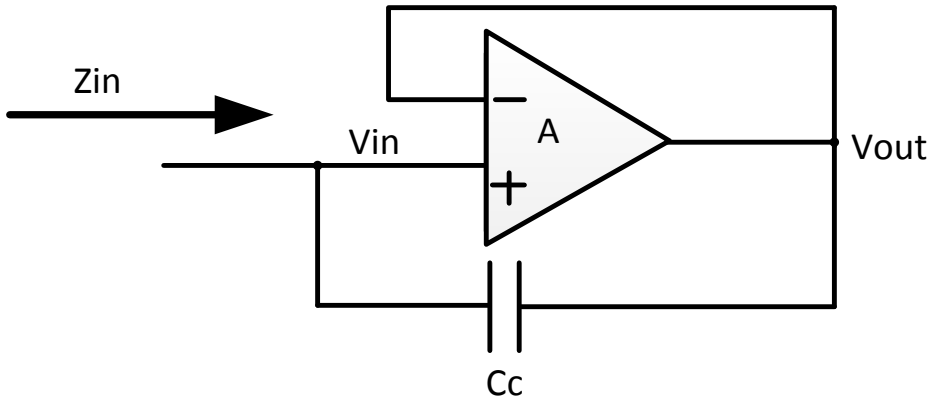


Fig. 4.9 Bootstrapped circuitry showing the suppression of the coupling capacitance through the tracking amplifier

## 4.5 Circuit Implementation of The Oscillator

Fig. 4.10 (a) shows the design of the CDS oscillator for the proposed bootstrapped correlated-double-sampling (BCDS) sensing system. The nature of self-capacitance touch sensing prefers a single-ended capacitance-modulation action as opposed to a differential implementation. In addition, the limited gain and bandwidth of the bootstrapping amplifier requires a sinusoidal waveform instead of a square wave to avoid performance deterioration due to poor waveform replication at higher harmonics. Unlike a traditional LC single-ended oscillator, where there is a large on-chip or off-chip passive element (such as the off-chip inductor used in [19]), the BCDS sensor employs an inverter-based active resonator similar to that reported in [28]. The right four inverters I2,I3,I4,I5 construct an gyrator to form an equivalent active inductor, while the left inverter (I1) serves as a negative resistor to provide energy to the resonator. The equivalent small signal mode of the circuit can be derived as Fig. 4.10 (b) with a corresponding oscillating frequency derived as (12)

$$Z_g(s) = \frac{V_A}{g_{m5}V_B} = \frac{sC_2}{g_{m5}g_{m3}} \tag{10}$$

$$L_e = \frac{C_2}{g_{m5}g_{m3}} \tag{11}$$

$$f = \frac{1}{2\pi\sqrt{L_eC_L}} = \frac{1}{2\pi\sqrt{L_eC_L}} = \frac{1}{2\pi}\sqrt{g_{m5}g_{m3}/C_LC_2} \tag{12}$$

Where $Z_g(s)$ is the Laplace transform of the input impedance of the gyrator, $C_L$ is the channel load capacitance and $C_2$ is a tunable capacitor array to alter the active inductor value so that the oscillator frequency can be varied.

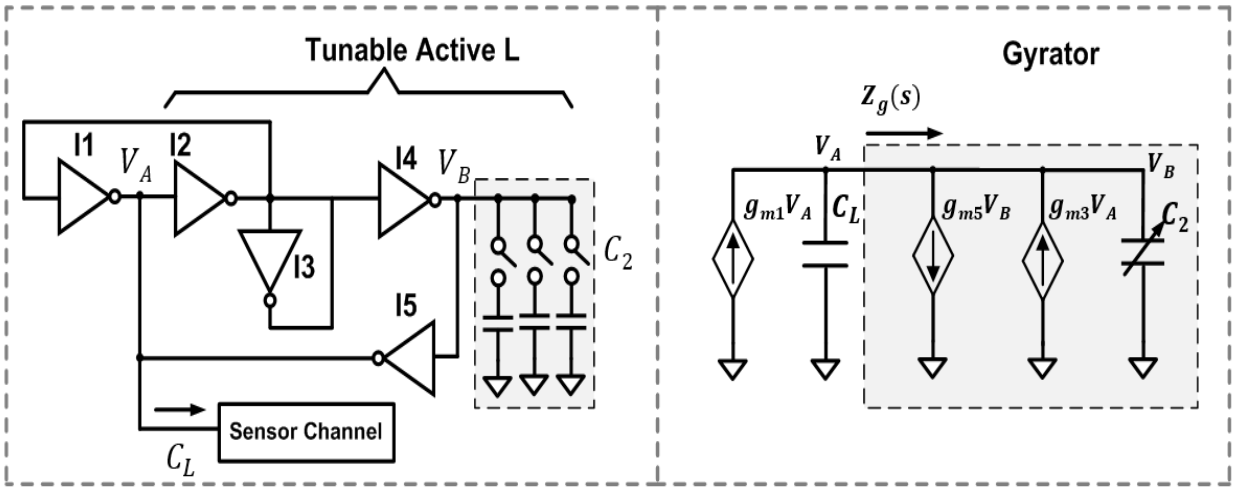


(a) (b)

Fig. 4.10 (a) Simplified schematic of the inverter based active resonator and (b) its corresponding small signal mode

To further ease the bootstrapping amplifier's design, reduce power consumption and improve the oscillator's linearity, diode clamps are paired with each inverter to reduce the voltage swing of the oscillator shown as Fig. 4.11.

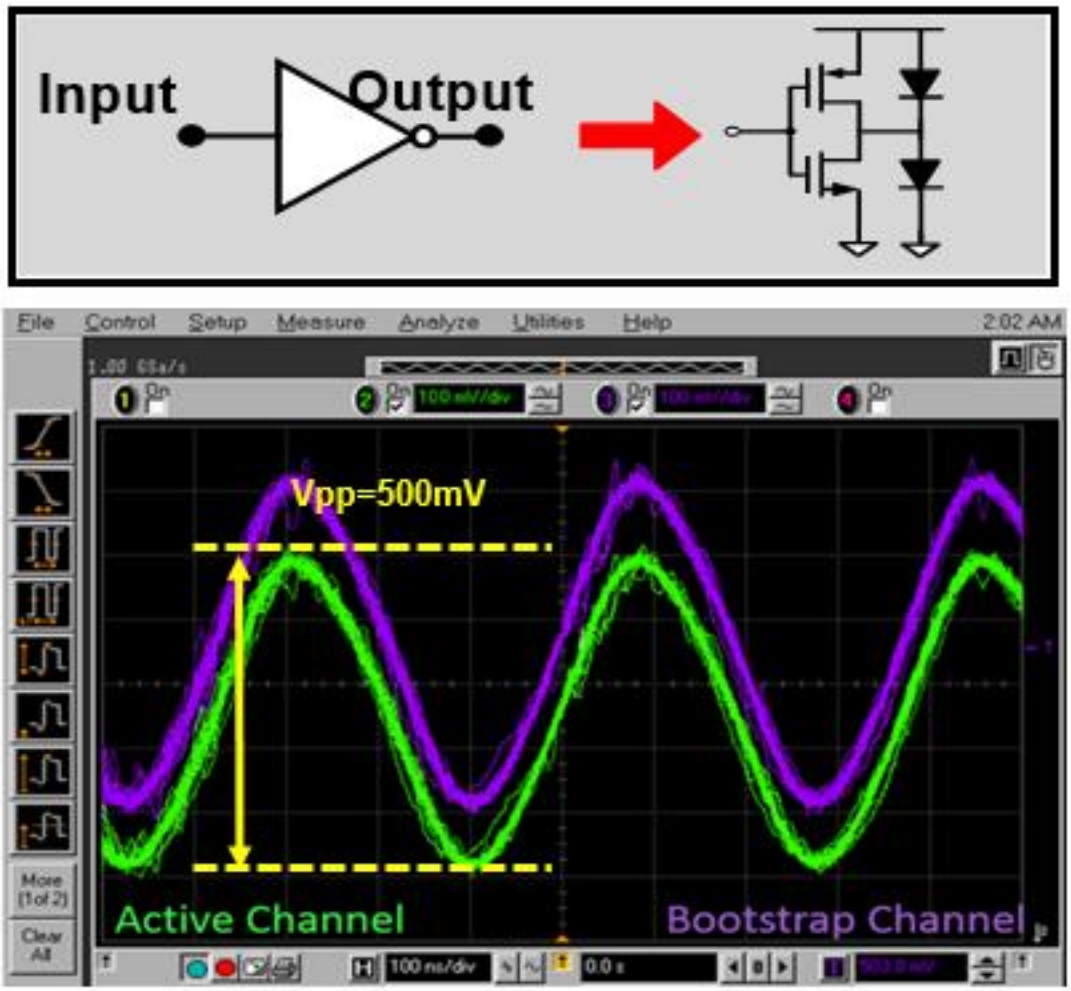


Fig. 4.11 Diode clamped inverter design and measurement of the oscillator signal in the active channel and the bootstrapped signal on an inactive channel

## 4.6 Digital core and USART Design

In order to calculate the sensed finger capacitive value of each channel and send the information to PC to do signal processing, a digital core with a USART communication block is designed. The digital core includes function control as well as the counter to do integration.

The USART is a serial-to-parallel interface inside the chip, which communicates with a microcontroller. The microcontroller works as a medium between chip and the PC. The handshaking operation between USART which serves as a slave and the microcontroller which serves as a master is shown in Fig.4.12.

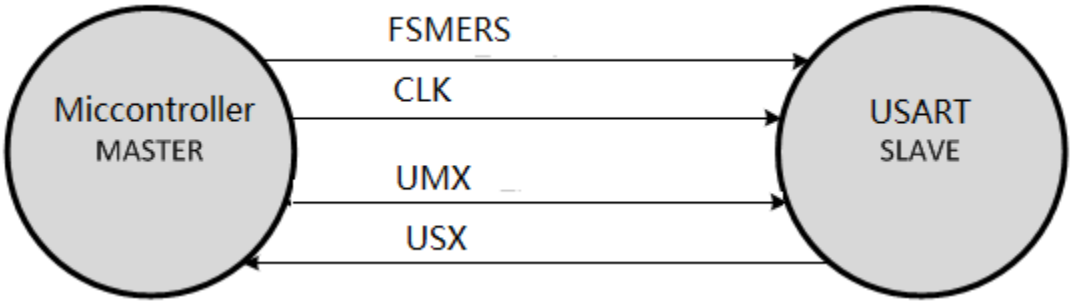


Fig. 4.12 USART and Microcontroller Handshaking Operation

The microcontroller initiates the communication by sending a “1” to USART through the wire UMX, and then sending the data through UMX port. The USART recognizes 1st “1” in the UMX which will be regarded as a ready signal of packet. Then it will keep receiving each bit. Once the USART finishes reading all the 41bit data, it starts to implement the functions. After another two clock cycle, it will begin to answer to the microcontroller which feedback 24bit data to microcontroller through USX and the microcontroller will transfer data to PC.

The counter is designed with a 16bit word length supporting integration up to 65536 clock cycle. Our oscillator runs at a few MHz frequency which can be fully covered by this integration range.

In additional to that, all the digital control regarding of the trimming caps and channel selection is through digital core, instructions are sent through PC.

The proposed hardware sensing circuit is fabricated through TSMC 65nm technology and the whole system occupy 1150um x 1800um area shown as Fig. 4.13. The hardware chip size is limited by the testing pads which can be removed in real production.

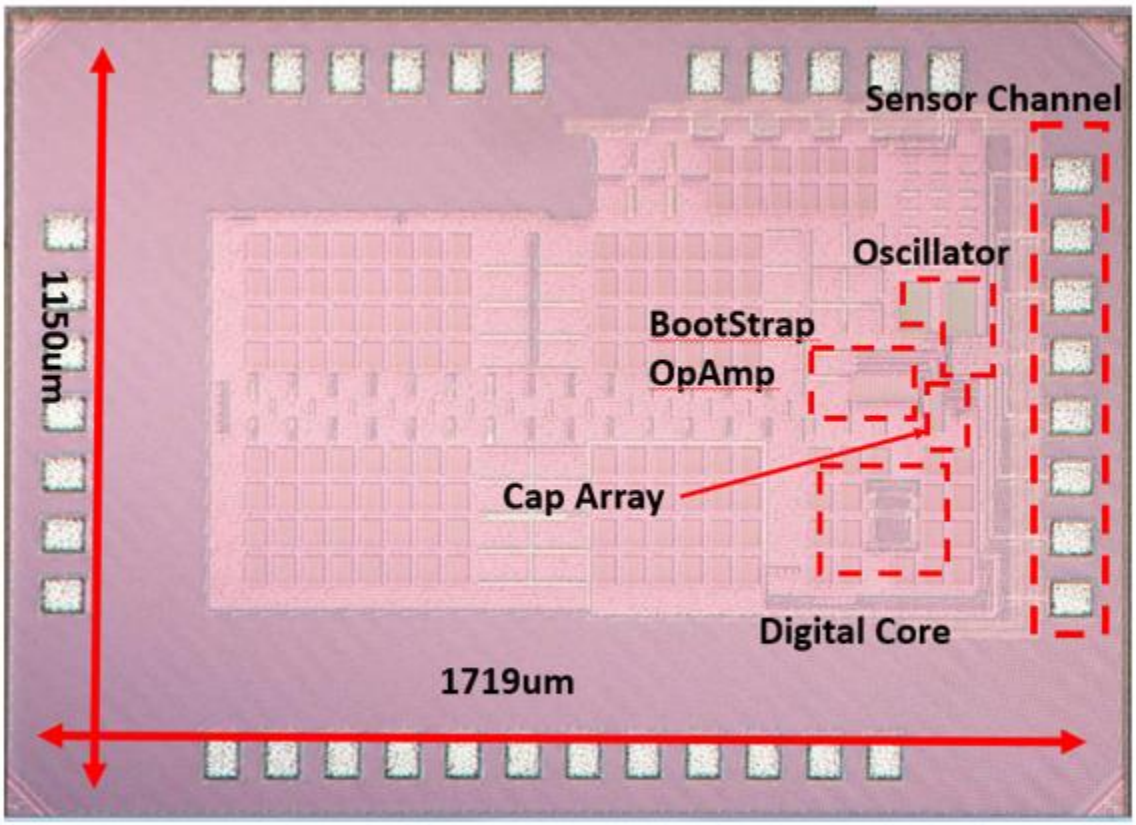


Fig. 4.13 Die photo of the touch sensor circuit

# CHAPTER 5 AIRTOUCH SOFTWARE ALGORITHM

In this section, we describe the algorithms that used to detect finger position detection. The whole backend digital processing procedures is shown in Fig. 5.1. The acquired channel's self-capacitance values first go to a group filter to remove noise effect and then the processed data will be used to calculate finger's instant X, Y, Z direction position separately. Finally, the instant position information goes to the reconstruction blocks to estimate the current finger position.

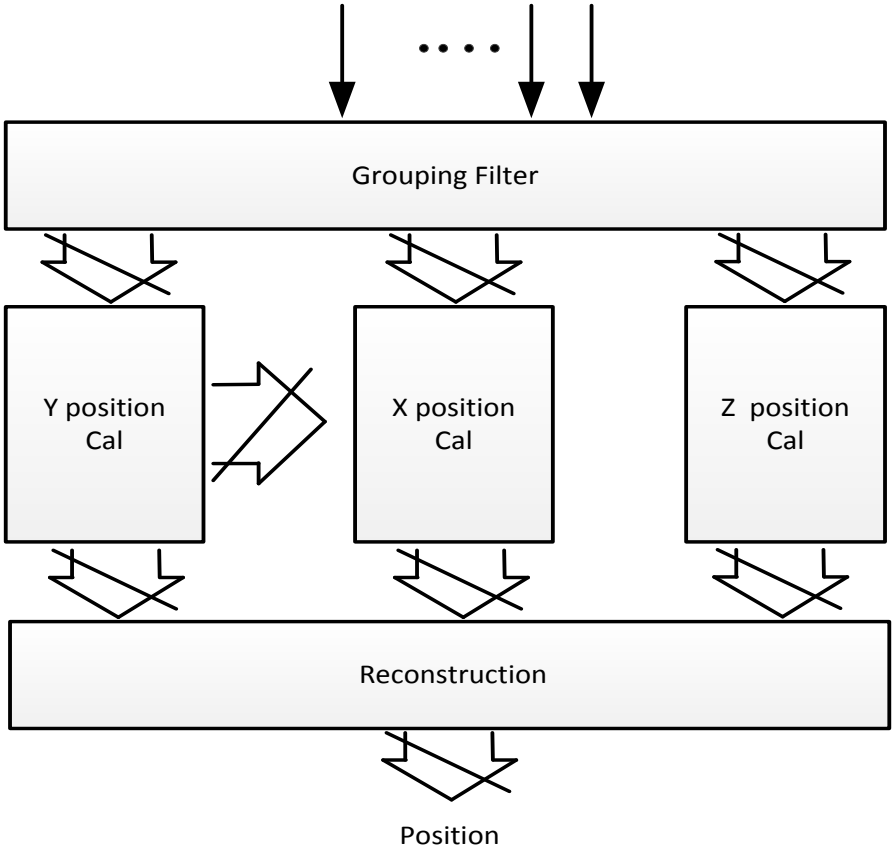


Fig. 5.1 Airtouch Signal Processing Procedure

## 5.1 Grouping Filter

As described in Chapter 4, the potential unwanted coupling capacitance of the touch panel can cause a system degradation, resulting an inaccurate finger position. Even the bootstrapping technique described before has cancelled the coupling capacitance mostly, a small fractional leaked capacitance can still create finger position error. In additional to that, the body-introduced background capacitance is also sensed during the scanning which creates ambiguity for the system to determine the real finger position. Fig. 5.2 shows how these two mechanisms affect the measurement of finger position. For example, when the finger is on top of the Channel 1 and 2, Channel 6 may see some fringe capacitance $C_{background}$ due to the hand shape and the coupled active $C_{finger}$ through $C_c$. This results in the inaccurate position estimation.

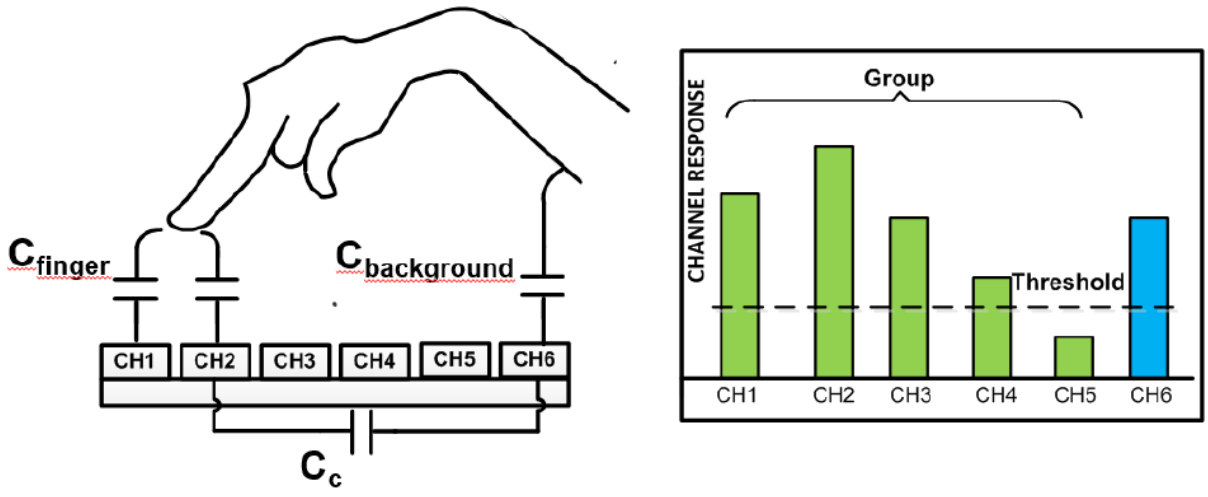


Fig. 5.2 Illustration of the grouping algorithm to filter out unwanted capacitive response

To avoid this, a grouping filter is proposed. The grouping filter categorizes the useful channel responses into a group and replace the unexpected response with its nearby channel response. The group filter is designed with the following steps:

1. Compare the maximum channel response with a pre-defined threshold to confirm a valid sensing.
2. Find the highest peak envelope of the channels' responses and group the corresponding channels.
3. The ungrouped channel’s response will be replaced with its nearby grouped channel’s response

After the grouping filter, the output data will be passed to each block separately to calculate the instant position in different directions.

## 5.2 Instant Y Position Calculation

The horizontal direction instant position estimation is separated into X, Y directions, the system first uses the grouped data to determine the instant Y position and then estimate the instant X position information through the obtained instant Y position information.

The instant Y position information can be obtained through comparing upper and lower channels' response difference. For a certain finger Y positions, the responses of these two different types of channels are different. For example, when a finger is close to the touch panel's upper edge, upper channels will have a much larger response compared to the lower channels due to its large sensing area compared with its nearby lower channel's. By assuming the finger induced capacitance value is proportional to its shielded area, we can derive the Y position through (13) (14).

$$r_{dc} = \frac{\sum \Delta C_{upper}}{\sum \Delta C_{lower}} \tag{13}$$

$$Y_{finger} = \frac{r_{dc}-1}{r_{dc}+1} Y_{max} = \frac{\sum \Delta C_{upper} - \sum \Delta C_{lower}}{\sum \Delta C_{upper} + \sum \Delta C_{lower}} Y_{max} \tag{14}$$

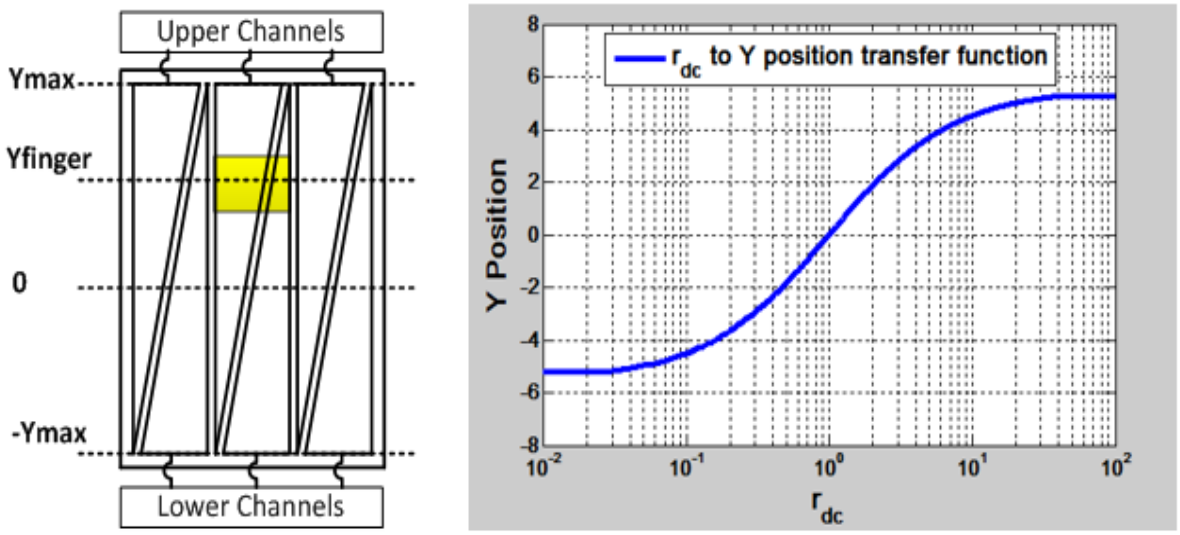


Fig. 5.3 Illustration of Y position calculation through linear modelling of the sensed capacitance: yellow area corresponding to finger position

However, this derived equations only fits when the finger capacitance can be modeled as a linear parallel plates' capacitance (sensed finger-capacitance is proportional to the shielded area). As the application aims to detect the finger position with a certain finger height, the induced fringing capacitance need to be accounted for. Fig. 5.4 shows how this fringing capacitance can affect the detection accuracy. Here, the center vertical arrows represent the linear finger-capacitance modeled as parallel plates' capacitance. In additional, the side surface of the finger also induced certain capacitance in the electrodes' input, causing a position error if using (14) to estimate.

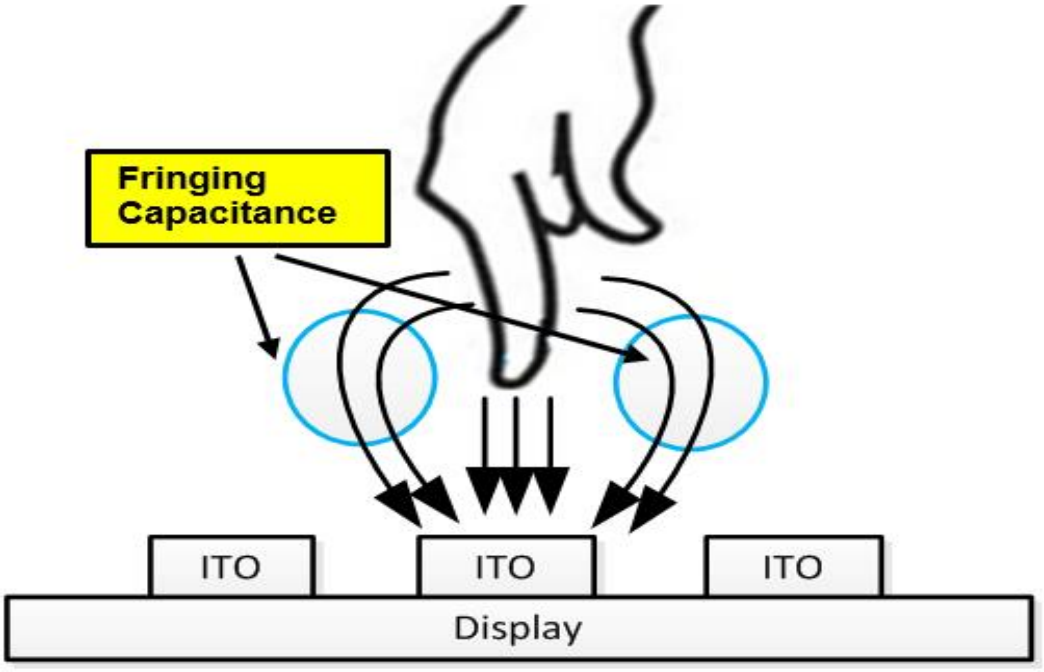


Fig. 5.4 Illustration of the fringing capacitance effect on the measuring accuracy

Since fringing capacitance is induced by finger's side surface, we have assumed the upper channels' sensed fringing capacitance is equal to the lower channels sensed fringing capacitance. In addition, we assume the fringing capacitance is fixed at a low finger height (<3cm). Based on this assumption, we can derive (14)'s error as (16). This added fringing capacitance generates a large position error when the finger is close to the panel's edge.

$$Y_{finger\_m} = \frac{\sum \Delta C_{upper\_m} - \sum \Delta C_{lower\_m}}{\sum \Delta C_{upper\_m} + \sum \Delta C_{lower\_m}} Y_{max} = \frac{\sum \Delta C_{upper\_l} - \sum \Delta C_{lower\_l}}{\sum \Delta C_{upper\_l} + \sum \Delta C_{lower\_l} + \sum C_{fringing}} Y_{max} \quad (15)$$

$$Y_e = \frac{\sum \Delta C_{upper_l} - \sum \Delta C_{lower_l}}{\sum \Delta C_{upper_l} + \sum \Delta C_{lower_l}} Y_{max} - Y_{finger\_m} = \frac{\left(\sum \Delta C_{upper_l} - \sum \Delta C_{lower_l}\right) C_{finging} Y_{max}}{\left(\sum \Delta C_{lower_l} + \sum \Delta C_{upper_l}\right)\left(\sum \Delta C_{lower_l} + \sum \Delta C_{upper_l} + \sum C_{fringing}\right)} \quad (16)$$

Here $\Delta C_{upper\_m}$, $\Delta C_{lower\_m}$ represents the measured upper and lower channels' sensed capacitance. $\Delta C_{upper\_l}$, $\Delta C_{lower\_l}$ represent the sensed linear finger capacitances of the upper and lower channels. $C_{finging}$ represents the sensed fringing capacitance in each channel.

To compensate this fringing capacitance effect in the position estimation, we add a fixed coefficient in the Equation. 14. The final equation is derived as (17) (18). To further verify the effectiveness of this coefficient on improving the detection resolution, an EM model of the finger and the touch panel is built with the Ansoft Q3D CAD tool as shown in Fig. 5.5. Simulated finger-induced capacitance values are put in (13) (14) to calculate the finger Y position and compare with the real position value in the EM modeling. As shown in Fig. 5.5, this added coefficient has improved the position estimation accuracy by 11dB compared to the reported work in [29].

$$Y_{finger} = \beta_0 \frac{\sum \Delta C_{upper\_m} - \sum \Delta C_{lower\_m}}{\sum \Delta C_{upper\_m} + \sum \Delta C_{lower\_m}} Y_{max} \tag{17}$$

$$\beta_0 = \frac{\Delta C_{upper\_l} + \Delta C_{lower\_l} + C_{finging}}{\Delta C_{lower\_l} + \Delta C_{upper\_l}} \tag{18}$$

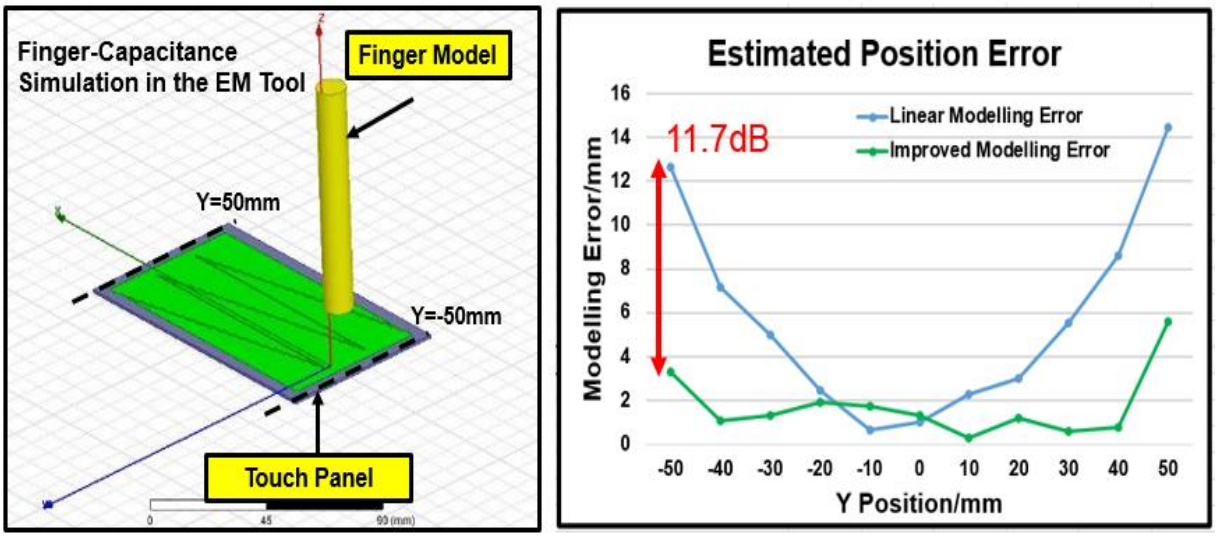


Fig. 5.5 Illustration of Y position calculation modelling and the comparison of the new proposed equations estimation error versus the old one

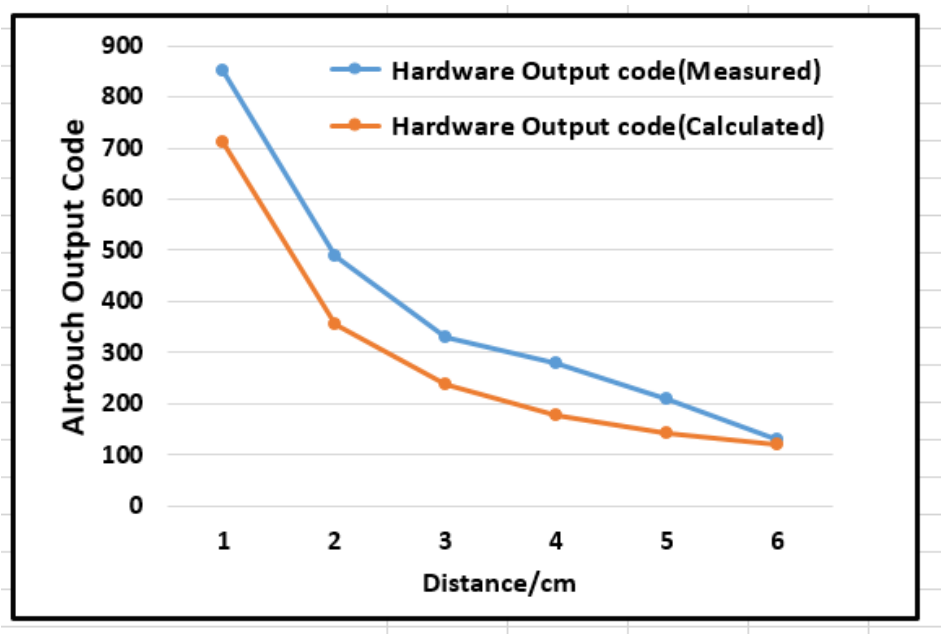


Fig. 5.6 Measured Airtouch output code versus the linear modelling calculated results

To further validate our assumptions about the fringing capacitance, we did a measure of the fringing cap value with the finger in different position. Fig. 5.6 shows the measured hardware output code versus the ideal calculated response (ignoring fringing capacitance effect). Fig. 5.7 is representing the difference of these two codes which represented the added fringing capacitance. As it shows, up to 4cm, the fringing capacitance adds between 100 to140 code on the final output. This variation is small compared with the finger capacitance response. So our assumption above regarding of the fringing capacitance effect and modelling is accurate enough for low finger height horizontal position detection.

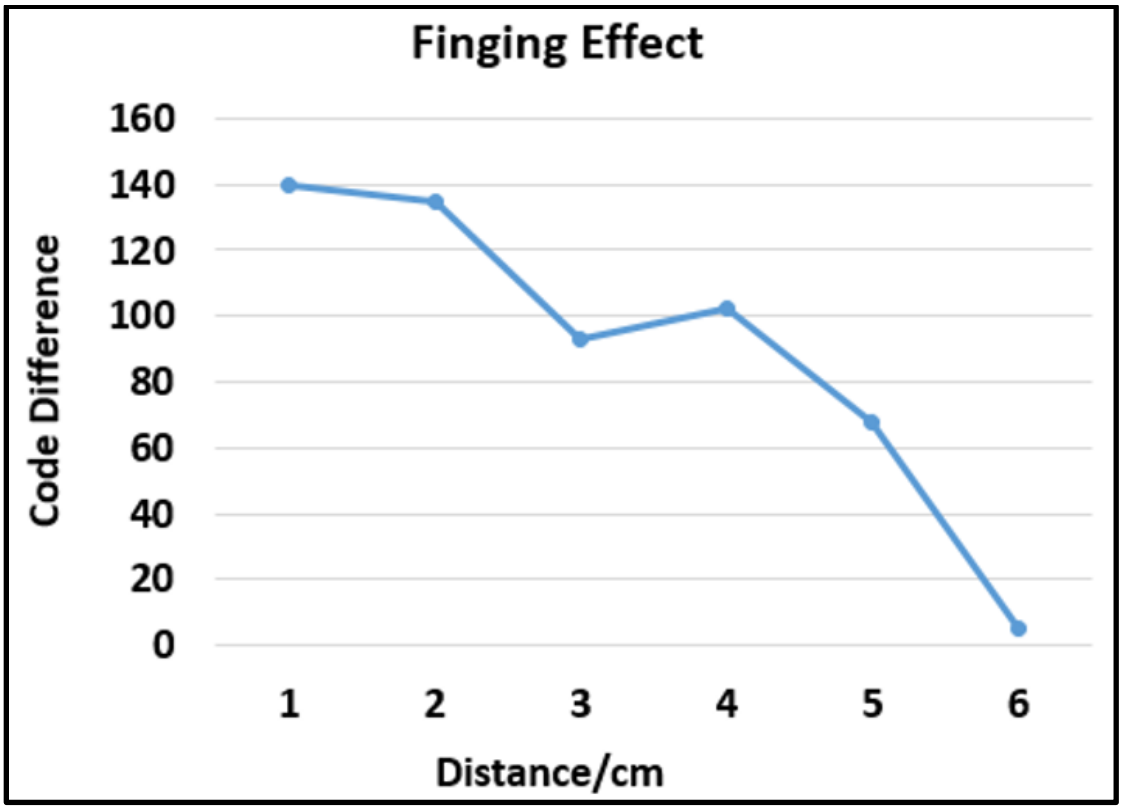


Fig. 5.7 Code difference introduced by fringing capacitance effect

## 5.3 Instant X Position Calculation

The instant X position is calculated based on the center-weighted algorithm. Noticing the electrode has different width in different Y position, so how to accurately represent the electrode's center position in X direction plays an important role to determine the actual finger instant position. Here we use the obtained Y position information to define each electrode's X direction's center position and calculated the finger position based on the weighted average of all the electrodes' center X positions. The algorithm can be separated into the follow two steps with the equation shown on (19) (20).

1. Find each electrode's center $X_{position}$ based on the finger's Y position obtained above
2. Calculate the weighted average of all the channels' center $X_{position}$ with their finger capacitive responses and output the average as the final X position.

$$X_{center\_i} = \frac{X_{top\_i}+X_{bot\_i}}{2} + \frac{X_{top\_i}-X_{bot\_i}}{2} \times \frac{Y_{finger}}{Y_{max}} \quad (19)$$

$$X_{finger} = \frac{\sum_i X_{center\_i} \times \Delta C_i}{\sum_i \Delta C_i} \quad (20)$$

Here $X_{center\_i}$ is the i channel's center $X_{position}$ at the certain Y finger value and the $X_{top\_i}$ corresponds to the i channel's top-edge's middle point X position; $X_{bot\_i}$ represents the i channel's bottom-edge's middle point X position and $\Delta C_i$ is the sensed i channel's finger capacitance. These parameters are explained Fig. 5.8.

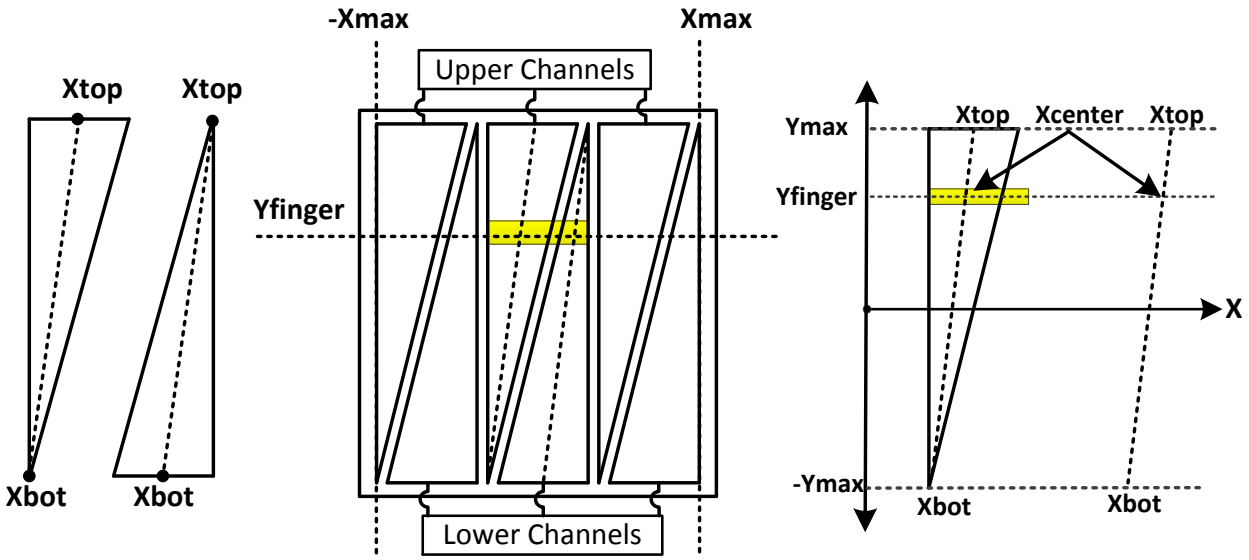


Fig. 5.8 Electrode's center position calculation at a certain finger Y position

## 5.4 Instant Z Position Calculation

The instant Z position calculation is based on the total measured finger-induced coupling capacitance on the touch panel. As the size of the touch panel is much larger than the user's finger, the finger is modeled as a small circular disk on top of the plane. In this case, the coupling capacitance is a combination of the parallel coupling capacitance and fringing capacitance. Here the parallel coupling capacitance is inversely proportional to the finger height, while the fringing capacitance has a non-linear transfer function at a large finger height [30].

To obtain an accurate relationship between the capacitance and finger distance, we have used the polynomial curve to fit the EM simulation results on the finger height versus channel's sensed finger capacitance. Since the application is targeted to be embedded in mobile phones where computational resources are limited, we have removed the 3rd and above orders to reduce the computation complexity. The Z direction equation can be written as (21):

$$Z_{finger} = a + \beta_0 \frac{\varepsilon_0 A}{\sum_i \Delta C_i} + \beta_1 \left(\frac{\varepsilon_0 A}{\sum_i \Delta C_i}\right)^2 \quad (21)$$

where $a$, $\beta_0$, $\beta_1$ are constant coefficients obtained through curve fitting on the EM modelling result, while $A$ represents the finger surface area and $\Delta C_i$ corresponds to the i channel's sensed finger capacitance. In real application, we also adjust the coefficients a little through fitting on the experiment results.

Here the finger is modelled as a 10cm height grounded-cylinder with a diameter of 1cm as Ref [31]. The screen is modelled as a glass covered by ITO. The sheet resistance of the ITO is

defined as 140Ohm/square. The finger modelling is an approximation compared with real finger in real-world scenery. However, considering the target application is for near screen detection (finger to screen distance <6cm) and the limited computation ability of the mobile CPU, we believe this is an appropriate modelling for the Airtouch design.

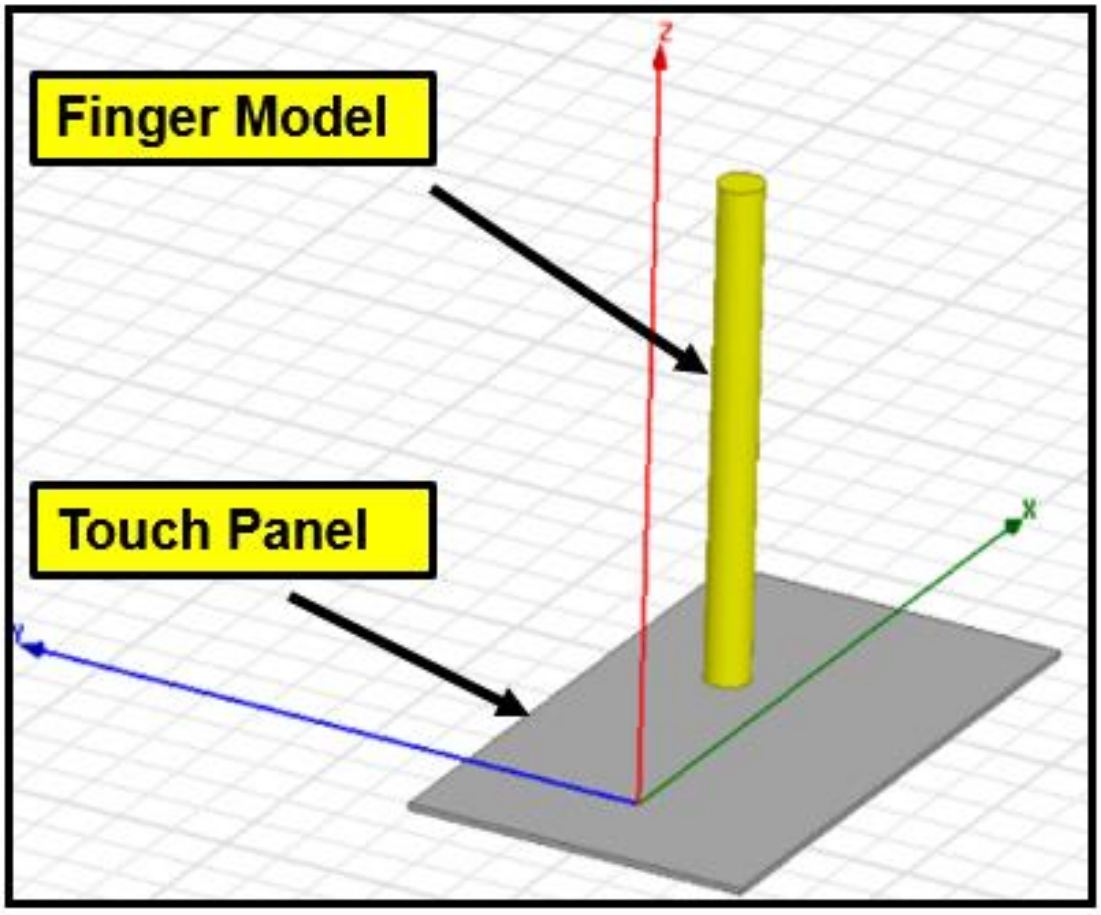


Fig. 5.9 Modeling of the Finger and Touchscreen in the EM Tools

To verify the effectiveness of this equation to estimate finger's Z position, we have put our modeled finger and touch panel in the EM tools and simulate the electrode's capacitance response with the finger in different horizontal positions (left, center and right) and different heights. The obtained capacitance derives the estimated Z position through (21) and is compared with the real finger position in the EM tool. Results are summarized in Fig 5.10 below. As it shows, the estimated error of this modelling is less than 4mm for up to 6cm finger-height.

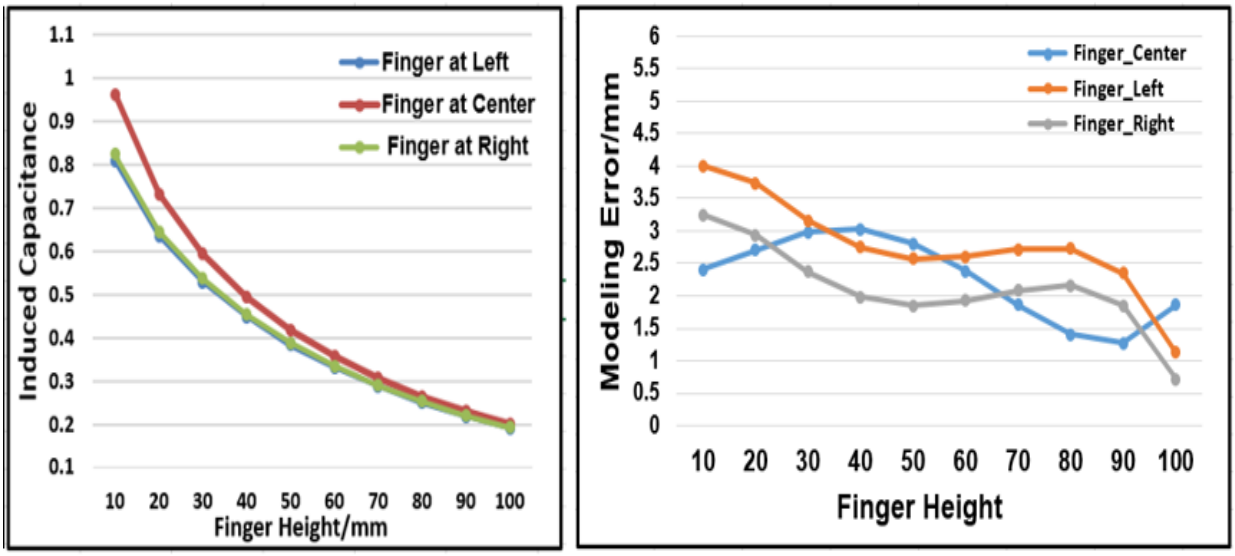


Fig. 5.10 Finger Position Estimation Error in Z directions

## 5.5 Position Reconstruction

The final reconstructed finger position is based on the instant finger position information obtained from above. Since the finger is remotely to the screen, any environmental or systemic noise can result a large variation on the calculated finger position, making the output finger position unstable. In addition, the environment can also generate some random peak noise due to the electromagnetic interference or background change, causing a large finger position jump from sample to sample.

To avoid this, a 5th order IIR filter has been implemented on the reconstruction block to remove random peak noise effect as well as stabilizing the reconstruct finger position. The final position is based on an average of the 4 previous results plus the calculated instant position information. The filter equation is shown in (22). Through using this IIR filter, high frequency noise is removed and output position change is much smoother.

$$P[n] = a_1(P[n-1] + P[n-2] + P[n-3] + P[n-4]) + a_2 P_{instant}[n] \quad (22)$$

$$a_2 = 1 - a_1 \quad (23)$$

Where $P[n]$ represent the final position currently, and $P_{instant}[n]$ represented the instant position calculated through the above model. $a_1, a_2$ are constantly coefficient to adjust the weight between instant information and previous result.

The software graphic interface is shown in Fig. 5.11. On the right side, there are four buttons for different function calls. Initialization is used when first launching the system and this function will setup the PC and Airtouch SOC's interconnections. Calibration function is used to calibrate each channels' load to the same property as described before, after that, the user can click

Start button to initiate the Airtouch 3D touch detection and Stop button is for closing the application when finished the demonstration. The detected finger position is shown on the left plot.

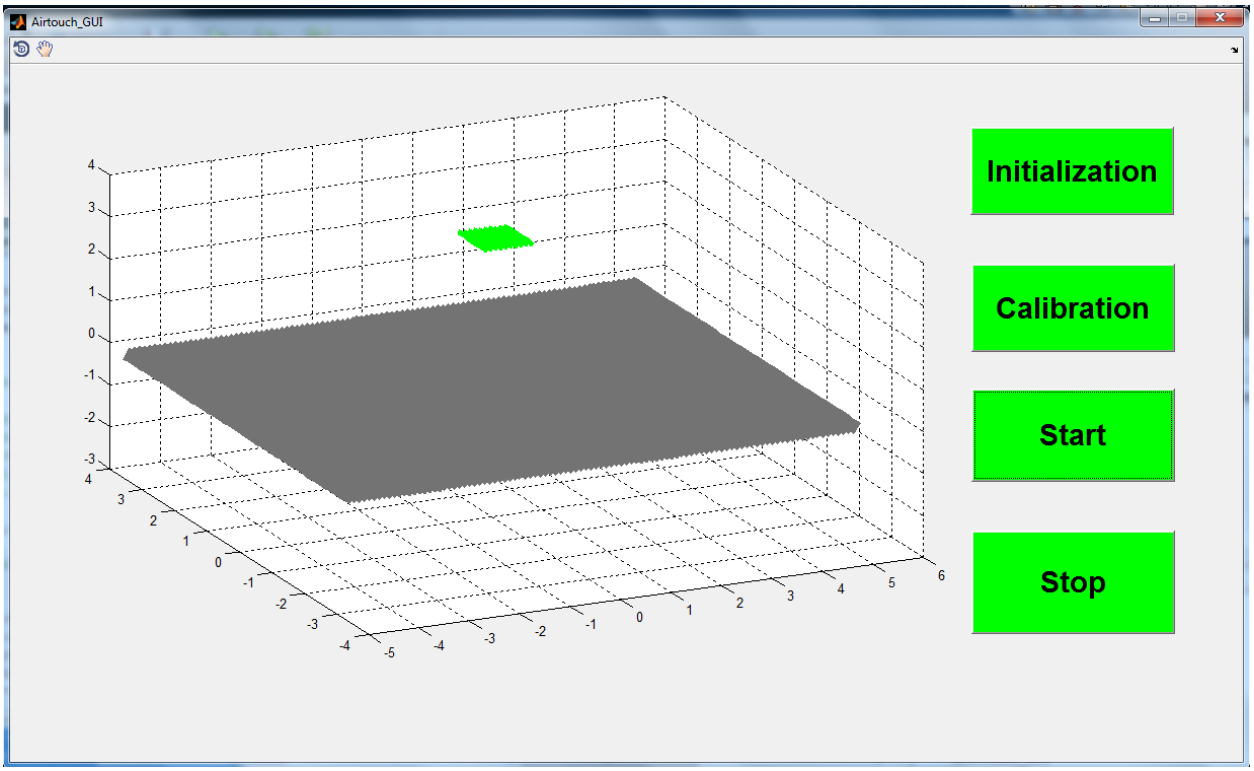


Fig. 5.11 Airtouch Software GUI Interface

# CHAPTER 6 AIRTOUCH SYSTEM PERFORMANCE EVALUATION AND APPLICATIONS

In this section, a prototype of the proposed Airtouch 3D touch sensing system has been built and measured. The first experiment is to check the CDS method in improving the system sensitivity. Then, a comparison of the channel response to different finger position is listed to prove the reduction of the inter-channel coupling effect through bootstrapping technique. After that, the system estimated position accuracy is characterized through experiment. Finally, a new Airtouch 3D sensing system platform has been built and characterized with instant video demonstrations of the system's concept.

## 6.1 Hardware Circuit Measurement

### 6.1.1 Oscillator-based-CDS Performance Evaluation

As described in Section II, one of the techniques we implement to improve the hardware sensing resolution is by applying CDS method to reduce the noise in the system. To verify the effectiveness of this method, we connected the prototyped sensor with a standard HTC 3.4" mobile touch screen array (Channel Number: X=16 Y=10). The synchronized scope capture of the active channel and idle channel's response is shown below with finger on or not on top of the screen.

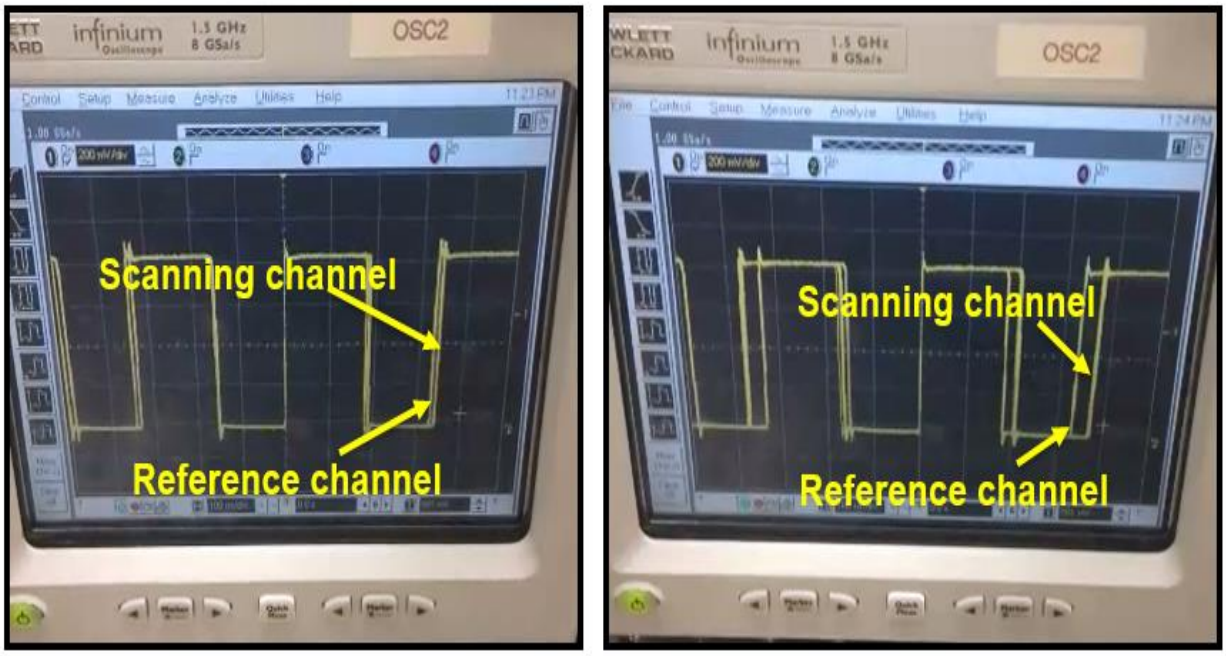


(a) (b)

Fig. 6.1 (a) channel response with no fingers and (b) channel response with fingers on the top

In addition, we have also used the scope to measure the active resonator's phase noise which is a critical parameter to evaluate the Airtouch system sensitivity. The measured phase noise is at 1MHz and achieves -123dBc/Hz as shown in Fig. 6.2

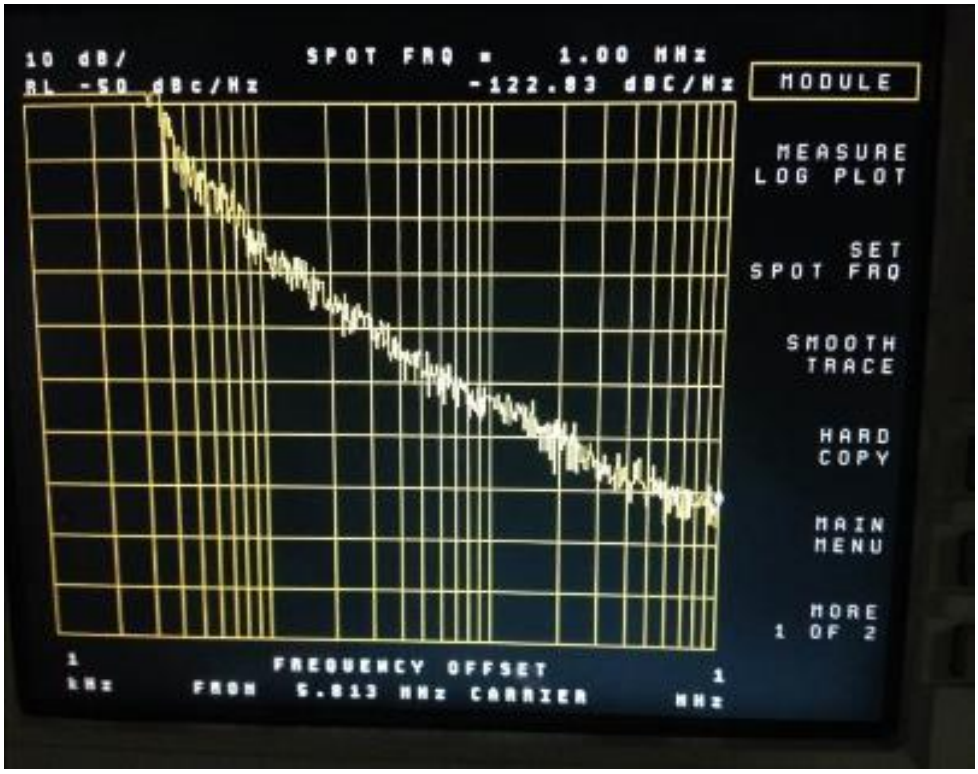


Fig. 6.2 Phase noise measurement of the Airtouch sensing oscillator

During the measurement, we first record the sensor's counter output when the sensor is connected to the reference channel (dummy load) and then repeat the measurement with the sensor connected to the active channel. Next, we plot these two cases' values and compute each case's standard deviation. Then, we perform the subtraction operation to produce the CDS output. Fig. 6.3 shows the counter output code for the regular channels as well as the CDS output. Based on the curve of the active channel's output and reference channel's output, we see a high levels of correlation between the two. By comparing the standard deviation of the regular channel output and the CDS output, we see 10.5 dB reduction of system noise through CDS function.

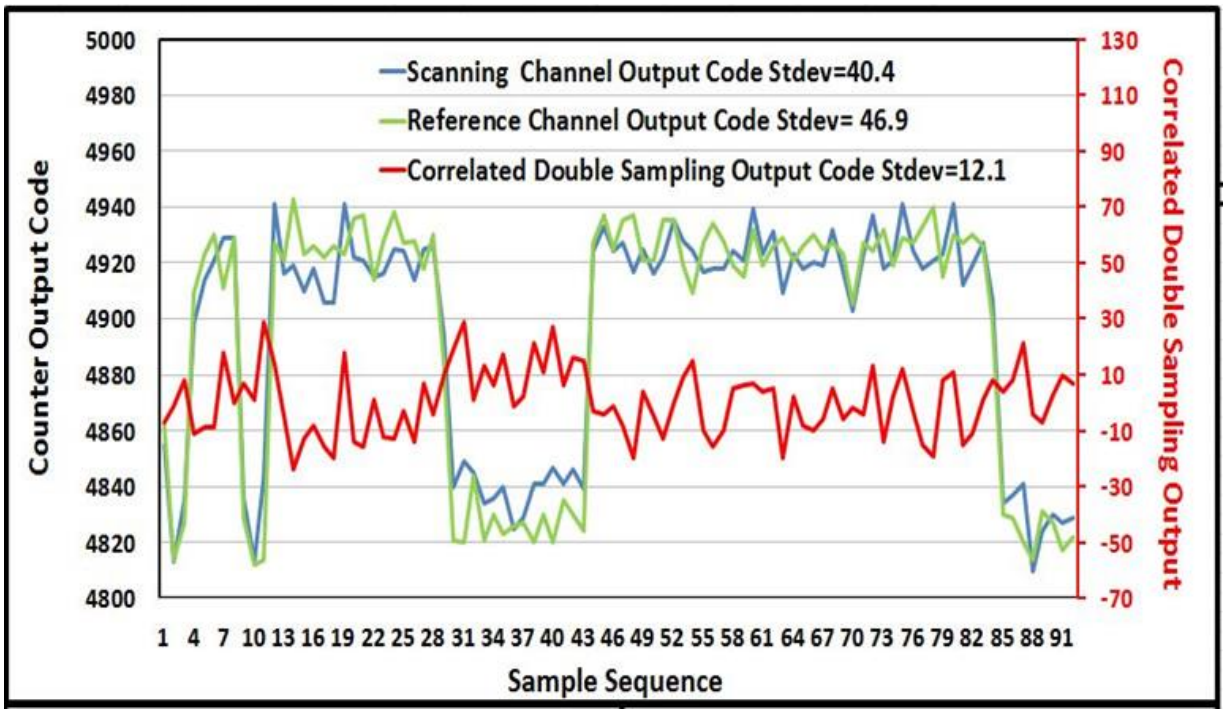


Fig. 6.3 Measurement of the counter output for the reference channel and an actively channel showing that the oscillator is correlated between both conditions

### 6.1.2 Bootstrapping Technique Evaluation

Besides the CDS, the bootstrapping circuitry is another technique we propose to reduce the inter-channel coupling effect to improve the hardware circuit resolution for finger position estimation in X,Y direction. To verify this, the sensed channel is fixed to a vertical channel located in the center of the screen. The finger is moving from the left side of the screen to the right side with different heights.

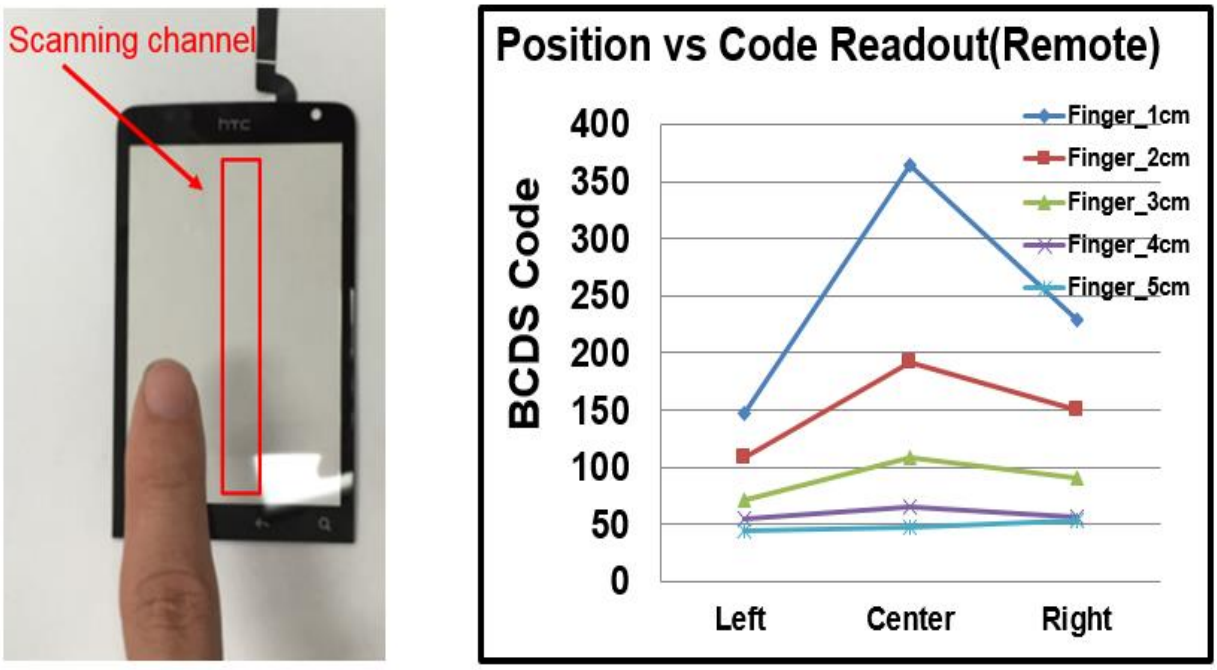


Fig. 6.4 Airtouch hardware output code versus finger position for different finger heights

The measured channel response is shown in Fig. 6.4. As it shows, when the finger's height is below 3cm, the bootstrapping circuitry provides sufficient coupling isolation, resulting a code difference to be comparable with the measured code result. When the finger is above 3cm, because of the limited gain of the amplifier and the reduction of the finger-induced capacitance, the sensor

responses among different finger positions are almost the same. In this case, the bootstrapping circuitry can no longer support the X direction position differentiation.

The whole hardware sensing system consumes a 2.3mA current at 1V supply. More than 80% of the current is consumed by the bootstrapping circuitry to drive the idle channel's parasitic coupling capacitance. The oscillation frequency is at a range of 1MHz-15MHz. Depending on the applications and the touch panel property, the system can tune its oscillation frequency.

## 6.2 Algorithm Performance Evaluation

The evaluation of the system's algorithm accuracy in finger-position estimation is conducted through a prototype setup as Fig. 6.5. The prototype system contains a mobile-phone-sized touchscreen with a triangular electrode pattern as described before, a low power capacitive sensing circuit to sense the finger capacitance, an ARM-based microprocessor unit (MCU) and a laptop to calculate and display the reconstructed finger position.

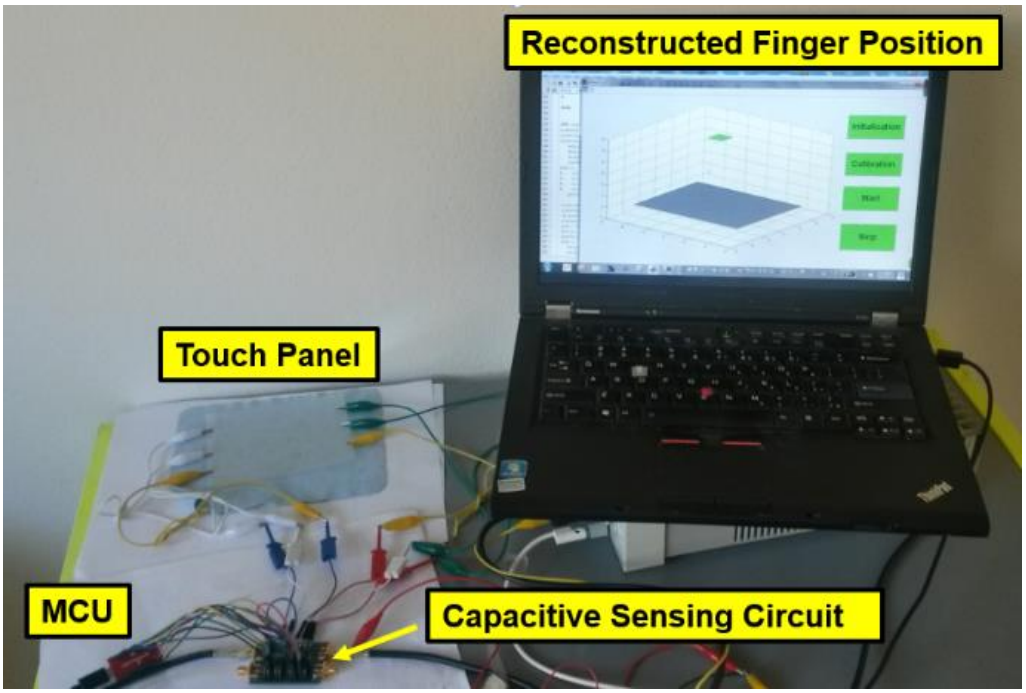


Fig. 6.5 Airtouch Demonstration Setup

The reconstructed finger position is represented as a $1cm^2$ green square in the coordinate system, while the touch panel is modeled as a grey rectangle with same size as the real panel. The system is real-time updated with a sampling speed up to 30 times per second. The experiment is conducted with user's finger hovering on top of the screen and moving both horizontally and

vertically. Fig. 6.6 compares the real finger position in the space with its reconstructed value in the Airtouch system. Specifically, Fig. 6.6 (a), (b) shows finger at different corners of the touch panel with a height of 1cm. The corresponding detected results is shown in (e) and (f). Another comparison shown between (c) and (d) is about the Z direction detection resolution. In (c), the finger is at about 4cm above the screen while in (d) it is 0.5cm to the screen. The raw video of this performance evaluation is [31] while the reconstructed position is shown in [32]

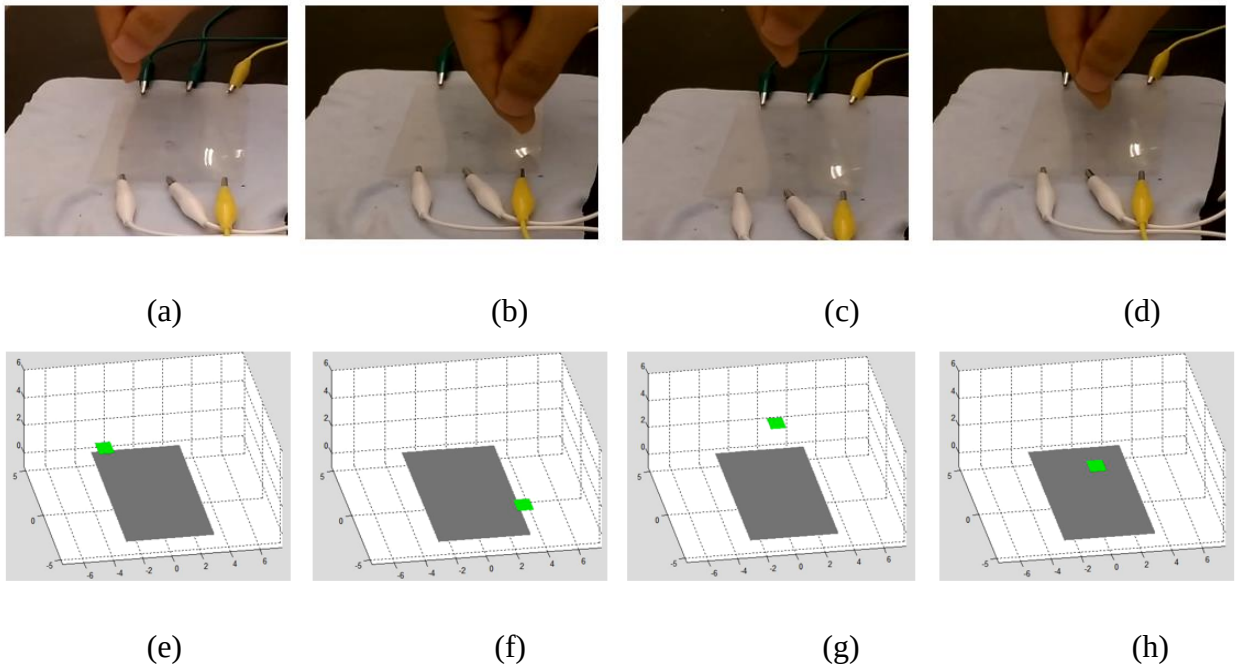

(a) (b) (c) (d)

(e) (f) (g) (h)

Fig. 6.6 Comparison of Airtouch Sensing Result versus real Finger Position. (a), (b), (e), (f) is the finger horizontal moving comparison. (c), (d), (g), (h) is the finger vertical moving comparison

The experiment shows that the system achieves an X, Y direction resolution up to 0.6cm (measured at a finger height at 1cm) through the improved algorithm to reduce the fringing capacitance effect. The horizontal direction resolution reduced when finger height is higher and achieves no differentiation if finger height is more than 4cm. Experiment shows this resolution reduction is mainly coming from two factors:

1. Weak finger-induced capacitance causes the channel-coupling effect dominated and results no channel response difference for different finger positions.

2. As the finger height increased the finger fringing capacitance becomes dominated and makes the proposed position estimation model inaccurate.

In addition, the system achieves a Z direction detection range up to 6cm with a resolution of 1.5cm. The detection error in Z direction is more than the modelling predictions at a large Z distance. Through experiment, we believe this is mainly caused by simplifying the surrounded environment (i.e. hand shape, body shape) in the EM modelling.

Table II lists the performance summary of the Airtouch system and comparison with other relevant work. Compared to other relevant work, the Airtouch system shows to be more suitable for mobile device where the power and space are limited.

TABLE II

PERFORMANCE SUMMAYR AND COMPARISON

| | ISSCC14 | MGC3130 | This Work |
|---|---|---|---|
| Sensing Type | 3D Large Screen | 3D Large Screen | 3D Mobile |
| Touch Layer No. | 2 | 2 | 1 |
| External Component Required | Yes(33uH inductor) | No | No |
| Screen Size | 30cm x 40cm | 14.8cm x 9.9cm | 10cm x 6cm |
| Height Resolution | 0.7cm | X | <0.6cm@1cm Finger Height |
| Z direction detection range | 30cm | 10cm | 6cm |
| Power Consumption | 19mW | 66mW | 2.3mW |
| Die Area | $4.2mm^2$ | X | $2mm^2$ |
| Supply Voltage | 1.2/2.5V | 3.3V | 1V(sensing circuit) 3.3V(MCU) |

## 6.3 Airtouch System Demonstration

To further validate our concept of implementing this technology into mobile devices to provide advanced user-experiences, we built a mobile-prototype platform with our Airtouch system integrated as shown in Fig. 6.7. Here, the screen is fabricated through depositing ITO on top of plastic PET film. The screen size is characterized as 10cm × 6cm, integrated together with the Airtouch SOC through the PCB board.

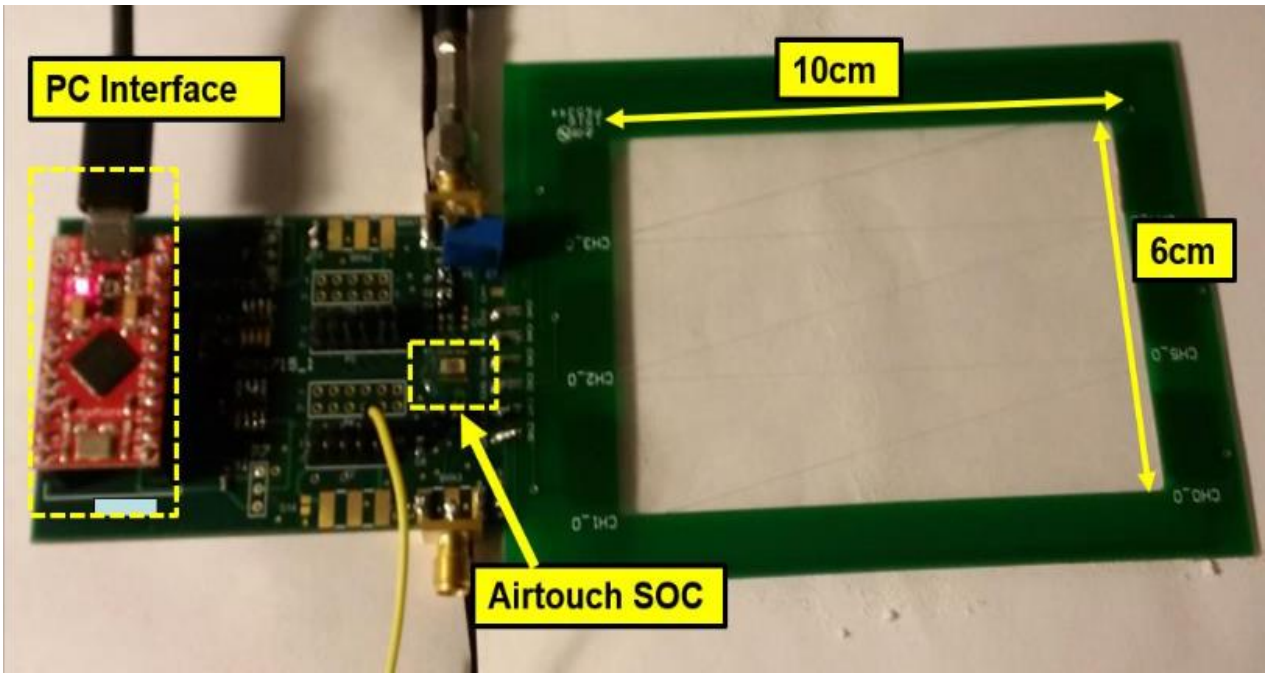


Fig. 6.7 Airtouch Mobile-Prototype Platform Setup

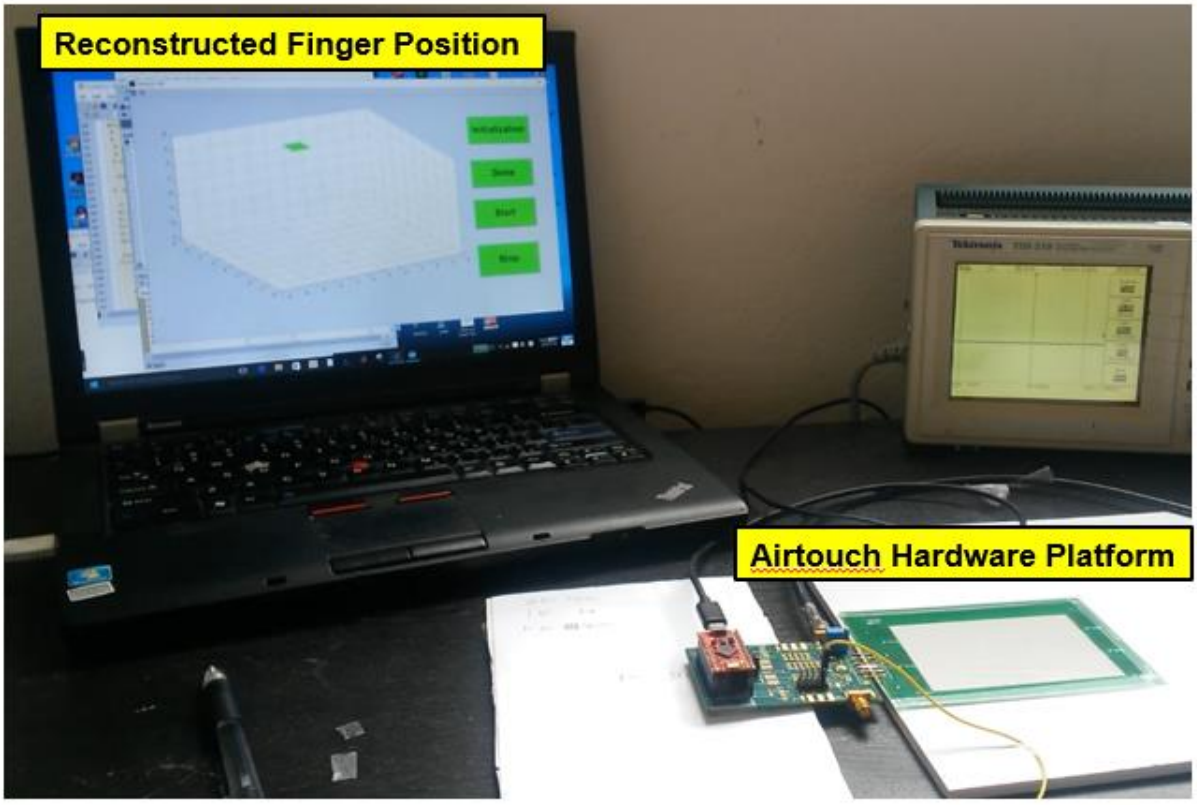


Fig. 6.8 Airtouch Mobile-Prototype Platform Demo Setup

The 1st synchronous demo video for single-finger position capture is shown in [33]. The demonstration begins with charactering the finger horizontal position detection accuracy at a certain finger height (2-3cm). Next, we perform some simple gestures by drawing circles on top of the screen to characterize the system's responding speed to dynamic finger movement. Finally to verify the Z direction detection range, the finger is moved up and down on the screen with a range up to 6cm. As shown in the demonstration video, the prototype platform can capture the user's finger movement on top of the screen successfully through the Airtouch sensing system.

The 2nd synchronous demo video characterizes the system performance to muti-finger position detection as shown in [34]. Specially, in this case, we target two fingers' position detection. As shown in the demonstration video, the system can successfully detects the two-

finger's movement in both X, Y, Z direction separately without generating any diagonal ghost point. In addition, we have found the multi-finger position has a limited resolution compared with the single-finger position detection due to the background effect of the hand shape. To further improve multi-touch detection accuracy, a more complicated finger modelling for multi-touch detection is required.

As demonstrated, the Airtouch system offers the potential to improve traditional 2D mobile touch sensing to 3D sensing. The demonstrated system focuses on detecting the 3D finger position and user's gestures with existing mobile hardware device. While this prototype employs a customized hardware sensing circuit, it can be replaced by any existing high resolution capacitive sensor (e.g. [35]).

## 6.4 Airtouch System Applications

Unlike 2D touch sensing, the Airtouch System offers a much better user experience through detecting finger movement in space. Advance mobile games/ applications can be realized through using this new feature. Here we are proposing several potential applications that can benefit from this technology.

**1. Motion tracked mobile games**

As the mobile games industry become more and more competitive, the video game company are more interesting to provide the game in a way that can interact with users, not through key board typing or mouse clicking, but more complicated interaction like motion tracking or voice recognitions. Microsoft's Kinect [36] is an example which involves users in front of the TV and tracks the user's motion change through camera. When merging this technology into the mobile devices, the camera solution for motion tracking is not suitable and efficient any more. This is mainly due to the following reasons:

(1) Changed background environment of the mobile screen makes the vision detection difficult. Unlike TV application where the place is fixed, mobile phone's application can be at any place and even a moving environment. In this case, the camera can certainly detect the background change in front of the screen and false recognize as a motion. In other words, the vision recognition is not accurate without a stable background environment [37].

(2) Much higher power consumption through vision detection. As we pointed out in the introduction chapter, the mobile solution always requires minimum power consumption due to the battery limitation. Video recording and computer vision

processing spends much more power than touch solutions. Even using the best state-of-art mobile phones like Iphone 6s, the continuous video recording time cannot be more than 4 hours [38].

On the contrary, for Airtouch, which senses body induced capacitance, a stable background is not necessary. In addition, the power consumption is only 2.3mW. Compared with regular mobile battery capacity (usually 3600mAH), this is a negligible power consumptions. By combining the machine vision and Airtouch sensing, we can merge this motion tracking games into smart mobile devices and providing a better user experience in playing the video games.

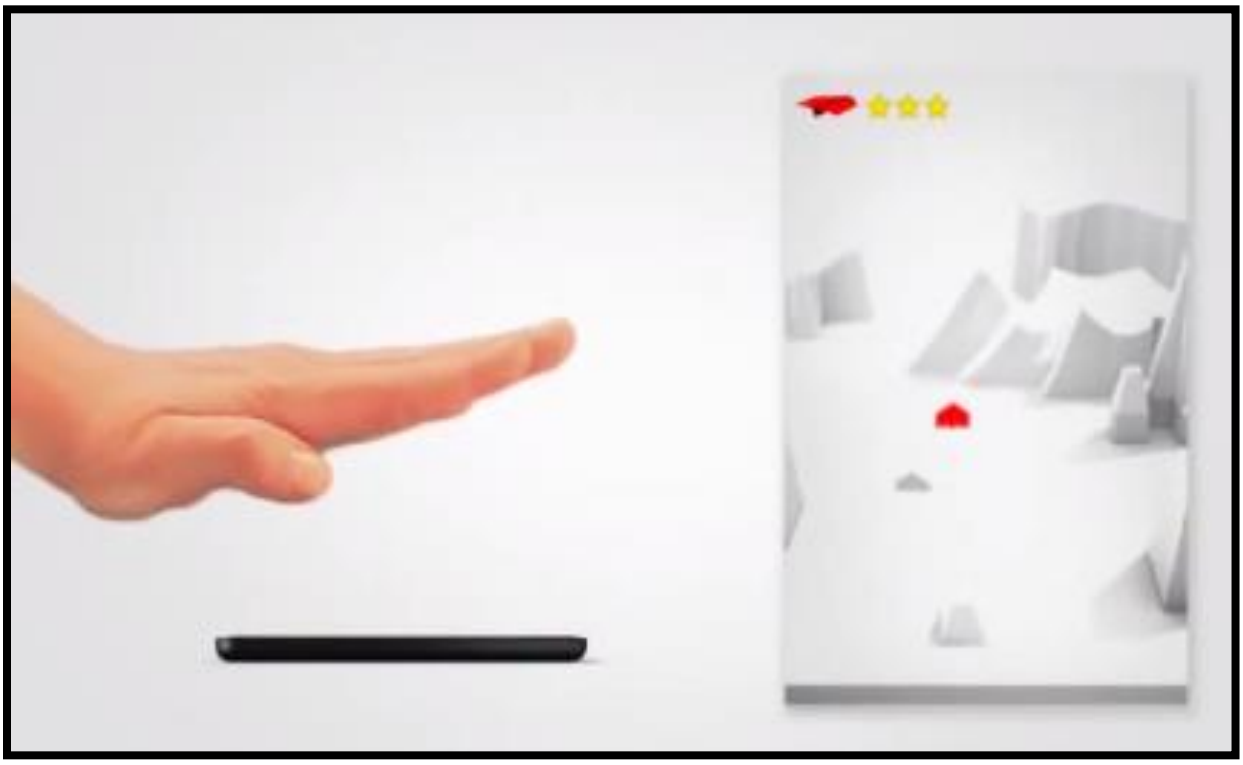

Fig. 6.9 Example of motion track games

### 2. Remote function control in mobile device

Besides the motion track games, the remote function control also becomes possible by implementing Airtouch technology in the mobile phones. In life, we have certain cases which we need to turn off/on the mobile applications but cannot touch it closely. For example, when users are driving, it is very dangerous to look at the screen and click the screen. On the other side, if we have certain device that can detect the gesture from the user, then we can use this gesture recognition function as a way for HMI. In this case, we can easily safely manipulate our phones during driving.


Fig. 6.10 Example of remote function control in mobile device

### 3. New human machine interface for wearable device

In addition to the application in the mobile device, wearable device can also benefit from this technology. As we saw, the wearable device is becoming more and more popular in our daily life. Most wearable devices' sizes are much smaller than the mobile phones ( i.e smart watch, Fitbit Surge). Currently, the interactions between the user and this type of devices is still through touching. However as the screen size kept shrinking, this communication is become more and more difficult and inefficient. On the contrary, the 3D touch sensing is not just limited to the physical screen size, it provides another dimension detection and through this added dimension detection, we have broaden the way of interfacing with the device and it can solve the interface limitation in the current small-sized wearable device. For example, instead of clicking the tiny button on the Apple watch, one can give a rising hand gesture on top of the screen to control the watch.


Fig. 6.11 Example of using 3D touch as a new interface between user and wearable device

# CHAPTER 7 CONCLUSIONS AND FUTURE WORK

While the touch screen has been widely implemented in the mobile product nowadays, the sensing range is still limited into two dimensional. Users are required to touch screen to communicate with the device. In this dissertation, we propose a completed new mobile touch sensing solutions: Airtouch, which can extend the mobile screen sensing range into three dimensional. The Airtouch system is aimed at detecting the user's finger position in space up to 6cm finger-height (distance between finger and the screen) and consumes comparable low power as the regular mobile touch sensor. In addition, this system is designed to be compatible with existing mobile screen environment. By achieving this, we wish to incorporate this technology into future mobile devices without sacrificing the existing mobile touch screen performance. The key contributions made in this work are as follows:

1. A single layer touch panel pattern design is used to implement 3D single/multi-touch sensing. This new touch panel only has one-layer electrodes to sense finger capacitance. In addition, manufactory cost is expected to reduce through using single-layer touch panel instead of traditional two-layer touch panel.
2. An oscillator-based correlated double sampling capacitive sensing circuit is invented. This sensing circuit can detect finger capacitance change in femto farad level.

3. Bootstrapping technique is first implemented in the touch sensing system and successfully eliminate touch electrode's inter-channel coupling. The horizontal resolution is improved by using this technique.
4. An inductor-less resonator as the sensing block in the system which provides large manufactory cost reduction.
5. Relative algorithms to estimate accurate finger position in space are proposed. Prototype system demonstrates that it can detect finger movement in a vertical direction up to 6cm and achieve a horizontal resolution up to 0.6cm at 1cm finger-height.

The proposed Airtouch system is not limited to mobile device applications though it has been validated as a mobile device HMI interface. Other applications such as Smart TV [39], tablets can also benefit by implementing this technology to improve their user experience. Moreover, emerging wearable devices can also benefit from this technology by implementing the gesture recognition on their small displays.

The further work of this project should carry on how to further improve the system finger position detection accuracy at a large Z distance. The current modelling between the finger position and the sensed capacitance is based on EM modelling and empirical formula. Recent research shows that machine learning is becoming more and more widely used in the object detection. As the finger is more far from the screen, the capacitance-to-position mapping is more complicated and non-linear. We found it is not easy to find a simple equation to represent these mapping. On the contrary, machine-learning has its property to auto-detect the input and output mapping relation through training. A primary experiment has been conducted using support vector regression with

this Airtouch platform to detect finger position in large Z distance. Through experiment, we find it provides a better position estimation compared with our analytic model result when finger is far from the screen (>3cm). So we believe it is a good future research direction for this project.

# REFERENCE


[1] http://www.techopedia.com/definition/19781/human-interface-device-hid

[2] I. Statista, "Global shipment forecast for touch-screen displays from 2012 to 2016, " Link: http://www.statista.com/statistics/259983/global-shipment-forecast-for-touch-screen-displays/

[3] K,-D.Kim et al., "A capacitive touch controller robust to display noise for ultrathin touch screen displays," IEEE International Solid-State Circuits Conference 2012, pp.116-117, Feb 2012

[4] H. rae Kim, Y.-K. Choi, S.-H. Byun, S.-W. Kim, K. Ho Choi, H.-Y. Ahn, J.-K. Park, D.-Y. Lee, Z.-Y. Wu, H.-D. Kwon, Y.-Y. Choi, C.-J. Lee, H.-H. Cho, J.-S. Yu, and M. Lee, "A mobile-display-driver IC embedding a capacitive-touch-screen controller system," in IEEE ISSCC Dig. Tech. Papers, Feb. 2010, pp. 114–115.

[5] P. Koundinya, S. Theril, T. Feng, V. Prakash, J. Bao, and W. Shi, "Multi resolution touch panel with built-in fingerprint sensing support," in Design, Automation and Test in Europe Conference and Exhibition (DATE), 2014, March 2014, pp. 1–6.

[6] Steve Kolokowsky, Trevor Davis, "Understanding Touchscreen Technology and Design" Cypress Semiconductor Corp.

[7] L.T Huang, "Oscillator-based Touch Sensor for Mobile Applications"

[8] L.Du, "Oscillator-Based Touch Sensor with Adaptive Resolution"

[9] Resistive touch Screen for Human/Machine Interface, VIDISONIC

[10] Analog Touch Screens application node of hantornix

[11] Resistive Touchscreen Introductions, https://en.wikipedia.org/wiki/Resistive_touchscreen

[12] Ik-Seok Yang and Oh-Kyong Kwon, "A touch controller using differential sensing method for on-cell capacitance touch screen panel systems," IEEE Transactions on Consumer Electronics, vol. 57, no. 3, pp. 1027-1032, 2011.

[13] The Working Principle of Capacitance Touchscreen, Onetouch technologies

[14] Touchscreen," Link: https://en.wikipedia.org/wiki/Touchscreen#Projected_capacitance

[15] Diffused Illumination, " Link: http://wiki.nuigroup.com/Diffused_Illumination

[16] Ian Maxwell. An overview of optical-touch technologies. Information Display, 23(12), 2007

[17] Introducing the NextWindow 1900 Optical Touch Screen: A NextWindow White Paper," Link: http://walkermobile.com/NextWindow_1900_White_Paper.pdf

[18] Comparing the Top 5 Touch Screen Technologies," Link: http://abraxsyscorp.com/blog/comparing-the-top-5-touch-screen-technologies/

[19] Microchip, "mTouch Projected Capacitive Touch Screen Sensing Theory of Operation".

[20] YZ. Hu; LC. Huang; WR. Louis; JS. Robinson; S. Wagner, James C. Sturm, N. Verma, "3D Gesture-Sensing System for Interactive Displays Based on Extended-Range Capacitive Sensing," IEEE International Solid-State Circuits Conference, pp.212 - 213, Feb 2014.

[21] K,-D.Kim et al., "A capacitive touch controller robust to display noise for ultrathin touch screen displays," IEEE International Solid-State Circuits Conference 2012, pp.116-117, Feb 2012.

[22] Barrett, G. and Omote, R. "Projected-Capacitive Touch Technology. Information Display," (26) 3, 2010. 16-21

[23] HTC Salsa Phone Introduction," Link: https://en.wikipedia.org/wiki/HTC_Salsa

[24] T. Davis, Cypress Semiconductor, "Reducing capacitive touchscreen cost in mobile phones".

[25] Chunchen Liu, Meng-Che Tsai, "Self-capacitive touch panel" US Patent 13/968,527

[26] Z. Tan, S. H. Shalmany, G. Meijer, and M. A. Pertijs, "An Energy-E_cient 15-Bit Capacitive-Sensor Interface Based on Period Modulation," Solid-State Circuits, IEEE Journal of, vol. 47, no. 7, pp. 1703-1711, 2012.

[27] VLSI Standards Inc, ITO Sheet Resistance Standards," Link: www.vlsistandards.com/products/electrical/ito.asp?sid=86.

[28] Barthelemy, H.; Bourdel, S.; Gaubert, J.; Battista, M., "CMOS inverters based high frequency voltage controlled sinusoidal oscillator," IEEE International Conference on Electronics, Circuits and Systems, pp 490-493, Dec 2007.

[29] L. Du, C. Liu, A. Tang, Y. Zhang, Y. Li, M.-C. F. Chang " Invited - Airtouch: A Novel Single Layer 3D Touch Sensing System for Human/Mobile Devices Interactions," ACM/IEEE Design Automation Conference, (Jun 2016), Austin, TX Accepted.

[30] G. Carlson and B. Illman, "The circular disk parallel plate capacitor," American Journal of Physics, vol. 62, no. 12, pp. 1099{1105, 1994.

[31] S. N. Makarov and G. M. Noetscher, Low-frequency Electromagnetic Modeling for Electrical and Biological Systems Using MATLAB. John Wiley & Sons, 2015.

[32] Airtouch demo: Reconstrust model in the matlab," Link: youtu.be/vbecKVDV9v0.

[33] Airtouch demo with software interface," Link: youtu.be/x0xgKJwmGWU.

[34] Airtouch demo: single touch," Link: youtu.be/3ivwCi3E8Ig

[35] Airtouch demo: multi-touch," Link: youtu.be/0Ob_1cYKtyQ

[36] S. Xia, K. Makinwa, and S. Nihtianov, "A Capacitance-to-Digital Converter for Displacement Sensing with 17b Resolution and 20μs Conversion Time," IEEE International Solid-State Circuits Conference, pp. 198-199, Feb. 2012.

[37] Microsoft Kinect, " Link: http://www.xbox.com/en-US/xbox-one/accessories/kinect

[38] J. R. Pansare, S. H. Gawande, and M. Ingle, "Real-Time Static Hand Gesture Recognition for American Sign Language (ASL) in Complex Background," Journal of Signal and Information Processing, vol. 3, no. 3, pp. 364{367, 2012.

[39] How long can you record 4K video on the new Iphone 6s 128 GB, " Link: https://www.youtube.com/watch?v=ltxM1t9lRjg

[40] Samsung Smart TV Introductions," Link: http://www.samsung.com/us/experience/smart-tv/